# Application of satellite optical and SAR imagery for urban reconstruction monitoring and land-cover classification in arid areas

光学およびSAR衛星画像を用いた乾燥地域における都市復興モニタリングと土地被覆分類

January 2017

Seyed Omid Hashemi Parast

Graduate School of Engineering

CHIBA UNIVERSITY

(千葉大学審査学位論文)

# Application of satellite optical and SAR imagery for urban reconstruction monitoring and land-cover classification in arid areas

光学およびSAR衛星画像を用いた乾燥地域における都市復興モニタリングと土地被覆分類

January 2017

Seyed Omid Hashemi Parast

Graduate School of Engineering

CHIBA UNIVERSITY

# Table of Contents

# Acknowledgements

# Curriculum vita

# Education

1999 – 2002        Peyvand Adab, High School Diploma, Mathematics and Physics, Tehran Iran.

2003        Pre-university College, Ottawa Cultural Center, Ottawa, Canada.

2003-2006        Azad University, Associate Degree in civil, construction, Roodehen, Iran.

2006-2009        Azad University, B.Sc. in Civil Engineering, South Branch, Tehran, Iran.

2009-2012        Tehran University, M.A. in Urban Planning, Iran.

2013-2017        Doctoral Student, Department of Urban Environmental Systems, Graduate School of Engineering, Chiba University, Chiba, Japan.

# Job experience

2005        MOSHANIR Consulting Engineering Company GIS research group intern member, water resources management for hydroelectric power plants.

2011        AZE PARDAZ KIMIA Co. Ltd Fulltime interior designer.

2012-2013        PAMCHAL construction Co. Engineer in planning projects and construction affairs.

2014-2015        Research Assistant (RA), Chiba University, Department of Urban Environment Systems, Graduate School of Engineering.

# Publication

1. "Monitoring and evaluation of the urban reconstruction process in Bam, Iran, after the 2003 Mw6.6 earthquake" Journal of the International Society for the Prevention and Mitigation of Natural Hazards, NHAZ-D-15-01558R1 2016

2. "Multi Parameters Golden Ratio and Some Applications" Applied Mathematics, 2011, 2, 808-816 Published Online July 2011 in SciRes

3. "Monitoring of urban reconstruction: a study of recovery process in Bam after the 2003 earthquake", S. O. Hashemi-Parast, F. Yamazaki, Proc. of the 14th Japan Earthquake Engineering Symposium, pp. 1139-1168, 2014.12

4. "Reconstruction monitoring of Bam city after the 2003 earthquake based on satellite images, statistical data and field observations", S. O. Hashemi-Parast, F. Yamazaki, The 5th Asia Conference on Earthquake Engineering, Taipei, Taiwan, 8p, 2014.10

5. "Study based on the causes and damages of urban noise pollution and public health." Accepted for oral presentation at The 5th Conference & Exhibition on Environmental Engineering, Tehran University, Iran, October 2011

6. "Optimum plastic waste management on the basis of urban environmental challenges and public health." Accepted for oral presentation at The 5th Conference & Exhibition on Environmental Engineering, Tehran University, Iran October 2011

7. "Evaluating the impact of biodegradable packaging on the municipal solid waste management to approach urban sustainable development." Accepted for oral presentation at The 4th Conference & Exhibition on Environmental Engineering, Tehran University, Iran October 2010

# Abstract

Investigating and understanding the reconstruction process and current situation of urban areas after natural disasters is a useful method for evaluating the performance of the project's implementers. In this study, we tracked and analyzed the reconstruction process in Bam, Iran, after the city was struck by an earthquake with a Mw of 6.6 on December 26, 2003. We adopted three approaches to assess the city's post-earthquake reconstruction comprehensively and to shed light on the progress and sustainability of disaster recovery projects. The results indicated that considerable progress had been made in reconstructing some of the damaged areas. However, progress was relatively slow in severely damaged areas.

Moreover, we detected and classified the recent land-covers of the Bam area by using the confusion of high-resolution synthetic aperture radar (SAR) Images (ALOS-2) and the optical image (Sentinel-2). Detection and Classification of land-covers by only optical imagery, in particular for buildings, are often complicated process with the low accuracy results in desert areas such as the Bam. We could obtain a reasonable classification of the land covers by the composition of quad- and dual-SAR images with reverse sensor's passes and normalized difference vegetation index (NDVI) from the Sentinel-2 Image. This method led to high accuracy, fast estimation and less dependency on visual inspection.

災害後長期間における都市の変化と現状の把握は，都市復興と発展を評価する重要な情報である。本研究は，2003年12月26日にマグニチュード6.6の地震が発生したイラン・バンム市の復興状況をモニタリングした。都市再建の過程を把握するために，3 つのデータを用いた。1 つ目は，政府が公開した統計データである。年ごとに統計された建物の数と材質の割合から復興プロジェクトの進行状況を評価した。2 つ目は，現地調査のデータである。2004，2007 と 2014 に行った3回の現地調査で撮影した写真を比較して，災害直後，3年後と現在における建物の変化を追跡した。3つ目は災害前後と現在の3時期に撮影された光学衛星画像である。衛星光学画像から復興による土地利用と土地被覆の変化を目視により抽出し，建物の被害レベルと比較して復興過程を評価した。これらのデータより，バンム市の復興に時間がかかっているものの，都市の再建に成功した。また，現在バンム市の都市利用を把握するために，高解像度 ALOS-2 の合成開口レーダ

(SAR)画像と光学画像を用いて都市被覆の自動分類を行った。砂漠とバンム市の建物が近似した反射特性を持つため，光学画像のみによる分類が難しい。そこで，撮影方向が異なる 2 枚の SAR 画像と併用し，バンム市内の都市被覆と周辺の砂漠の識別を行った。SAR の偏波情報から算出されたテキスチャ情報と光学画像から算出された正規化差植生指数(NDVI)を利用することで，高精度で土地利用を把握できた。

# Chapter 1

# Introduction

## 1.1 Background

Remote sensing and geographic information system are helpful and efficient tools in disaster management. Yearly, various natural hazards such as earthquakes, floods, landslides, tsunamis, volcanic eruptions, and hurricanes kill lots of people and destroy properties and infrastructures. Struggling with these hazards, the disaster mitigation communities and space technology work together in developing accurate and effective methods for avoidance, alertness and relief measures. Disaster prevention is a long-term process during which, Geographical Information System (GIS) is used for assessing the vulnerability and hazard risks by monitoring the land use changes.

The population growth and the over consumption of earth's natural resources have resulted in increasing defenselessness of our community and civilization to the natural hazards. Nowadays, remote sensing has made it possible for the professionals of disaster management to have effective project planning more accurate than ever before (Kundzewicz et al., 1993; Lanza and Conti, 1994; Sabins, 1986).

Preparation against disasters concentrates on predictions and warnings of imminent disasters. In this stage, information extracted from GIS, integrated with other relevant datasets, are employed for the design of disaster warning systems such as planning evacuation routes or establishing comprehensive emergency operations. Disaster relief takes place after and sometimes during the hazard. In this phase, GIS, in combination with GPS, is extremely beneficial in search and rescue operations in the areas that have been stricken by the hazard. By using the satellite technology, it is possible to recognize escape routes and locations for temporary settlement during and after the disaster.

Another important aspect concerning satellite monitoring involves assessment of the post-disaster recovery. Post-disaster recovery is the last phase of the disaster management cycle, which is often a lengthy, costly and complicated process (Van Westen, 2000). In this phase, satellite information is used for the evaluation of sites for reconstruction, mapping the environmental restoration and monitoring the reconstruction progress in the damaged areas. Post-disaster recovery is a primary phase in estimating the land cover changes and updating the database for prevention of similar damage in the future disasters (Hill et al., 2006). However, most of the disaster-related remote

sensing studies have primarily concentrated on the response phase of a disaster, and very few have considered the recovery phase as an element of the disaster management cycle.

From another point of view, the increasing numbers of the active satellites and their sensors have provided new opportunities to observe disasters on the Earth. The different types of spectral bands in visible, near infrared, infrared, short wave infrared, thermal infrared and SAR (Synthetic Aperture Radar) provides a sufficient spectral coverage and prepare incomparable data about characteristics of the Earth surface. Multi-dimensional computer enhancement of these data makes it possible to simulate the situation as accurately as possible and develop better prediction and monitoring models.

## 1.2 Objectives

The process of reconstruction is an important phase in the cycle of disaster management. Not only it provides accurate information about the post-disaster recovery process, but also it demonstrates the effort and progress that were made by a government or official organizations to alleviate the hardship of a natural disaster and meet the needs of survivors (Murao et al., 2013).

Therefore, investigating and understanding the reconstruction process is a useful method both for the management of the imminent hazards, as well as evaluating the performance of the implementers of reconstruction. On the other hand, official statistical data regarding reconstruction progress may not always be the most reliable data source for evaluation, because this information is usually collected by the same organization that was responsible for the execution of the reconstruction. Hence, remote sensing techniques and assessment of satellite images provide a direct, objective, independent, and more reliable method of evaluating reconstruction projects.

However, with all its benefits, monitoring land cover changes using remote sensing products is not a feasible task. Multiple methods should be used to extract and classify land use and land cover changes from a satellite data. Moreover, uncertainty can arise when dissimilarity of land covers in some areas confuse land-use classes. For example, accurate mapping of land cover changes is challenging in the arid and semi-arid environments due to the natural properties of these

environments. To that end, the fusion of optical and SAR satellite data merges more information from the image than optical pixel-based approaches, especially in urban regions.

The incorporation of spatial information provides high flexibility to the mappers. (Galletti and Soe, 2014). Particularly, in urban areas with spectrally similar or mixed classes, multiple sources with an efficient classification technique is required to derive reliable features for land cover mapping (Amarsaikhan et al., 2012).

With the introduction above, this study proposes two goals. First, to provide an evaluation of the post-earthquake reconstruction process in the city of Bam, Iran in a different time, and second, to introduce an improved classification method for detection of land cover changes in arid areas (such as regions in the city of Bam) by using a fusion of optical and SAR data. In this method, optical data are used to increase the effect of the vegetation in the SAR images and to allow for better classification of radar data (Chaouch et al., 2011)

## 1.3 Structure of the thesis

The goal of this thesis is to analyze the application of satellite optical and SAR imagery for urban reconstruction monitoring and land-cover classification in arid areas. The research is done in the subsequent chapters by first providing an introduction to the problems we are about to face. In chapter 2, deals with the basic concepts and state of the art needed to follow up next chapters. The third part covers monitoring and evaluation of the urban reconstruction process in Bam city, Iran. The fourth part deals with the application of quad- and dual-polarimetric SAR data combination for land-cover detection in desert areas. The general conclusions are drawn in the final chapter, which provides discussions obtained in this research. A flowchart of the methodology is presented in Figure 1.

```
┌─────────────────────────┐
│        CHAPTER 1        │──────◆ Overview of contents
│       Introduction      │
└─────────────────────────┘
             │
┌─────────────────────────┐
│        CHAPTER 2        │──────◆ Disaster monitoring
│  Preliminary Information │──────◆ Optical and SAR sensors
│   And Literature Review │──────◆ Land cover detection
└─────────────────────────┘
        │           │
┌──────────────────┐  ┌──────────────────┐
│    CHAPTER 3     │  │    CHAPTER 4     │
│ Urban Monitoring │  │ Land Cover       │
│ (Reconstruction  │  │ Detection        │
│ Process After    │  │ For Desert Areas │
│ Earthquake)      │  │                  │
└──────────────────┘  └──────────────────┘
```

Assessment of reconstruction ◆
Changes in land cover ◆
Changes in the buildings ◆

**CHAPTER 5**
**General Conclusions**

◆ SAR images fusion
◆ Optical and SAR images fusion
◆ Land cover classification
◆ Accuracy assessment

# Chapter 2

# Preliminary Information and Literature Review

## 2.1 Preface

In this section, we provide basic information on the major topics and techniques which used in this project. First, we briefly introduce remote sensing and its application for disaster monitoring and management. Next, we discuss land cover, land change science, and the use of remote sensing for detection of the land covers in drylands. Finally, we present classification schemes, algorithms, and image processing techniques.

## 2.2 Remote sensing and its application for disaster monitoring

Landsat 1, or "Earth Resources Technology Satellite 1", was the first satellite of the United States' Landsat program, since then we have come a far way with our recent advanced sensors with better spatial and temporal resolutions. Currently, many satellites and sensors provide comprehensive information about properties of the surface or shallow layers of the Earth. For example, thermal sensors measure surface temperature reflected from solar radiation and microwave sensors estimate the dielectric feature for determination of the soil surface humidity (Demircan et al., 1993).

With the aid of satellites as one of the key tools in the disaster management, the impact of natural disasters has been widely reduced. This is indebted to the disaster prevention (assessing the hazards and risks and planning the land use accordingly), with remote sensing techniques disaster preparedness (forecasting a potential hazard and delivering warning) and fast and proper disaster relief plan (OAS, 1990; UNDRO, 1991) all becoming possible with the sufficient attitude about the characteristic, anticipated repetition and intensity of a natural disaster, one can find favored approaches to mitigate the outcomes of these kinds of events.

In the cases of disasters that start very rapidly and affect large areas, such as floods or earthquakes, the use of synoptic earth observation methods has proven to be particularly efficient in the field of disaster management. Today, in most of the developed countries, where warning systems and building codes are advanced, remote sensing of the earth has shown the strong contribution to the prediction of disastrous events and thus saving people by delivering warning on time. Unfortunately, about 95% of the deaths caused by the natural disasters occur in the developing world, where a large proportion of the human population lives. Similar losses are expected in the

advanced countries, although with suitable disaster management strategies it is possible to minimize the harming consequences.

# 2.2.1 Brief Introduction to Remote Sensing

Remote sensing is the science of collecting, producing, and analyzing information about the Earth and earth-related phenomena with the application of sensors that do not come in contact with those phenomena (Buenemann et al., 2011). Sensors have the advantages that they provide non-biased information, can reach inaccessible and remote locations, and collect data on a regular basis (Jensen, 2005). Sensors come in various types including active or passive, sub-orbital or satellite. In active sensors, signals (such as sonar, laser, radio signals, etc.) are sent out to contact earth phenomena, and then the backscatters of those signals are recorded. In passive sensors on the other hands, electromagnetic radiation from sunlight that has been reflected or emitted from earth phenomena are recorded (Jensen 2005). Suborbital sensors fly on demand and collect data either actively or passively whereas, satellite sensors are orbit at a specific altitude and collect data passively on a regularly scheduled, tasked, or continuous basis once launched into space (NASA, 2007).

Hereafter, we only focus on the satellite sensors and provide some basic explanations about its resolutions. Remote sensing images obtained from satellite sensors are composed of a matrix of pixels laid out in a grid pattern. Pixels represent a particular area of the Earth surface and are square (Richards and Jia, 1999). A brightness value is assigned to each pixel in the image which corresponds to the amount of reflected or emitted energy/signal collected from the corresponding area of ground (Jensen 2005). Sensors acquire data at four resolutions: spatial, spectral, temporal, and radiometric. There are several definitions for spatial resolution, but typically it refers to the pixel size of a satellite image or the smallest feature that can be detected in it. The spatial resolution of an image is a function of the altitude that a sensor is located at and the area of the Earth's surface that the sensor can see at a given moment (Short 2010). Spectral resolution refers to the number and width of electromagnetic wavelengths detected by the sensor (Akasheh, Neale, and Jayanthi 2008). There are also sensors with a multispectral resolution that can detect several different

wavelengths (Jensen 2005). Similarly, there are sensors with a hyper-spectral resolution that can identify hundreds of narrow spectral bands (Short 2010).

The temporal resolution indicates the sensor's revisit time that is how often the sensor returns to the same spot on the earth. This ability of the satellite that can collect images from the same place over time provides opportunities to monitor changes occurring in a specific area of the Earth's surface. Lastly, radiometric resolution refers to the quantization level of the information contained in the pixels of an image. The higher the radiometric resolution, the more sensitive a sensor is to small differences in energy levels. Ranges correspond to the number of bits that are used to store data. Typical ranges are 8, 12, or 16 bits per pixel (Richards and Jia, 1999).

## 2.2.2 Land Cover Change Detection by Remote Sensing

Remote sensing has become an important tool in understanding landscape dynamics and the land change science (Ellis and Pontius 2010). There are two separate terminologies 'land use' and 'land cover' that are often used interchangeably. Land cover refers to the physical material at the surface of the earth, including vegetation, water, ground and other physical features of the land. It could also include human-made elements such as buildings, crops, etc. On the other hand, land use is characterized by the arrangements and activities humans undertake to modify a particular land cover type into build environments such as settlements and habitats (Rawat et al. 2015).

The land use and cover pattern of an area in an outcome of the natural and socio-economic factors as well as the extent of utilization by a man in time and space and therefore it has become a central element in monitoring environmental changes and managing natural resources (Zubair 2006). To that end, satellite imagery can provide spatially and temporally explicit and continuous information on both land use and land cover changes, which will help us, understand the direction and spatial extent of change (Buenemann et al. 2011, Elmore et al. 2000).

This quantified information on how land cover has changed over a period can facilitate the development of appropriate land management strategies (Houet et al. 2009). This is important because recent investigations indicate that land management practices are one of the most important factors influencing ecosystem structure and function (Chehbouni 2000).

Satellite imagery to land cover mapping has many useful properties. A large geographic area like ten thousand square kilometers can be covered by the synoptic view of the satellite sensor. Also, the data is collected in a spatially continuous fashion and regular basis, and it will be possible to be carefully compared with old data. Moreover, to facilitate the data analysis, they have been saved in digital format. There will be no need to digitize the analyzed information because the classified data are compatible with GIS. Also, many remote sensing data can often be downloaded without any cost, and land cover mapping can be performed at a very much low cost compared to other mapping methods. On the other hand, during the process field data collection can quickly become expensive in terms of time and labor.

Satellite imagery provides information where field work cannot be conducted for historical points in time and tends to be limited to point locations in small and accessible areas. Finally, the satellites can record data in the electromagnetic range beyond the visible spectrum as they have many sensors, which can detect things that are not visible to human eyes (Jensen 2005)

It should be noted that remote sensing and field work should be considered as two complementary approaches and although remote sensing has many advantages that fieldwork does not, fieldwork remains critical in the remote sensing process (e.g., calibration and evaluation) and the two approaches are not mutually separate (Buenemann et al. 2011).

## 2.2.3 Drylands Study via RS

Drylands are areas where water losses (such as evapotranspiration) exceed water gains (for example rainfall). Climatically it is defined as land surface areas where the aridity index –the ratio between the mean annual precipitation and mean potential annual evapotranspiration- is 0.05 to 0.65. Drylands cover about 40 percent of the Earth's land surface and are divided into three categories of arid, semi-arid and sub-humid. Monitoring the land surface changes in drylands provides information about desertification and land degradation in those areas.

Since drylands are usually vast and inaccessible, remote sensing has shown to be a useful and powerful mean for deriving information on soils, vegetation, and water resources, monitoring environmental changes, and assessing such issues as drought (Rhee et al., 2010), land degradation

(Albaladejo et al. 1998), and irrigated crop area (Beltran and Belmonte 2001) in those areas. In dry deserts, detailed pictures of dunes and other surface materials, and even surface features can be obtained (Nicholson, 2011). Although the resolution and accuracy of satellite images are still insufficient compared to other methods such as aerial photography and field observations, they still serve as an important mean for studying and monitoring inaccessible dry regions. In addition, remote drylands have, most of the time, a relatively clear sky (without clouds) and therefore the area is suitable for observation by optical sensors.

However, there are some challenges with satellite imagery of drylands that, if not attended, can lead to inaccurate assessment of land cover changes. These issues are usually due to natural characteristics of the vegetation cover (spectral and spatial sparseness), and the heterogeneity of surface features such as soil or urban surfaces in that area. Since satellite pixels are a combination of vegetation, soil, and other features, special techniques must be employed to unravel the different components within a specific area.

The remote sensing of vegetation cover is based on a physical principle that unlike other materials that show a gradual increase in reflectivity with wavelength, green vegetation shows a significant increase in the red and near-infrared wavelength (Nicholson, 2011). When surfaces are composed of a mixture of materials, they include a wide range of spectral profiles (Alberti, Weeks, and Coe 2004) and this could cause high reflectance in the thermal band and low reflectance in the near-infrared from these surfaces, which eventually leads to confusion in classification of lands with similar reflectance characteristics (Xu 2010).

 The secondary problem is due to the variation of soils regarding color differences. This is related to the soil biochemistry and its effect on the absorption of solar radiation. For example, rangelands are usually covered with bright soil due to its highly mineral ingredients, which makes it hardly detectable from barren agricultural fields. For the same reason, the spectral variability between the rangeland soil and regular ground complicates the classification event though both are from the same category (Elmore et al. 2000).

The third problem relates to the condition of mixed vegetation and bare soil, which causes multiple scattering. The low levels of biomass and sparse vegetation in drylands versus relatively high proportions of exposed soil make it difficult to detect different land cover types (Leprieur et al. 2000). The vegetation cover already reflects a significant amount of the radiation on the bare land.

Since the vegetation layer absorbs relatively more of the red wavelength than the near-infrared wavelength, the light that is scattered toward the ground is enriched in the near-infrared wavelength, hence, when reflected, it submits high values of vegetation index.

 The same problem may arise in the irrigated agricultural and riparian areas of drylands. In these regions that normally have an increased spacing of vegetation compared to non-arid regions, when the percentage of pixel occupied by canopy is reduced, the light is scattered by both vegetation and soil (Shupe and Marsh 2004). If the rate drops lower than 20 percent, Spectral discrimination of vegetation types becomes involved (Harris 2003).

Crop and fallow cycles can vary throughout the year and are often dependent upon irrigation schedules rather than rainfall. In drylands, spatial patterns consist of homogeneous grasslands, mixed shrublands, and even more various urban areas (Lo and Choi 2004), making a classification based on spatial pattern difficult.

The presence of non-photosynthetic vegetation that is common in these environments can also complicate the problem (van Leeuwen and Huete, 1996). Land degradation can further lead to a change in reflection properties due to decrease in vegetation cover, increase in erosion, and change of land surface characteristics (Escadafal et al., 2005). For example, the low density of vegetation in drylands means that in each pixel there is a very low percentage of land filled with a tree or a bush. This can allow the light scattered by soil overpower the vegetation signal leading to neglect of the vegetation part. Also, the physical features of dryland vegetation (which are usually small, sparse leaves, open crown, spine, thorns and photosynthetic stalks) decreases the difference between absorption in the red and reflection in near-infrared bands which is typically observed in green and leafy vegetation area. Therefore, detecting vegetation is more difficult in arid areas compared to other environments.

Even for a certain species, the classification of vegetation can become complicated because the spatiotemporal feature of the same specifics changes over time due to the topography and such events as fire or localized precipitation. The characteristics mentioned above make remote sensing of drylands and classification of different land cover types challenging. However, research has shown that combination of the various sensors and classifiers may help overcome some of these difficulties and provide a far more comprehensive survey of the observed area. In this investigation,

we evaluate the different combination of classifiers and present a new method for land cover detection in arid areas (Okin and Roberts 2004).

# 2.4 Image Preprocessing

All types of Satellite images, including captured by a multispectral sensor on a satellite or aerial photography in an aircraft, or any other platform, will have different geometric distortions. This problem is normal in the field of remote sensing, as we attempt to demonstrate the 3D surface of the Earth as a 2D image. All images from satellites are subject to some form of geometric distortions, depending on the manner in which the data was generated. There are numerous factors that can lead to these errors. Internal factors are introduced by the remote sensing system and include satellite and sensor calibration or equipment anomalies, the perspective of the sensor optics, the motion of the scanning system, the altitude, attitude and velocity of the platform, and motion of the platform (Shanker et al. 2006). Some external factors, which can cause distortions, are Earth's rotation, curvature, and terrain relief. Also, the atmosphere can play as another external error source by scattering and absorbing a proportion of the electromagnetic radiation as it passes to and from the target on Earth, hence impacting the signal that is received by the sensor. To improve the accuracy, such image distortions and atmospheric influences should be corrected before images are used for analysis and land cover classification (Song et al. 2001). Internal errors are systematic and predictable and therefore can be identified and corrected based on pre-launch or in-flight calibration measurements, whereas external errors require relating empirical ground observations to be corrected. Below, we discuss a few of these correction methods, including geometric correction, radiometric correction, and cross calibration.

# 2.4.1 Radiometric Correction

Radiometric correction is necessary to avoid radiometric errors or distortions and to ensure that terrestrial variables retrieved from optical satellite sensor systems are calibrated to a standard physical scale. (Teillet et.al 2010). When a sensor on board an aircraft or spacecraft observes an emitted or reflected electromagnetic energy, the observed energy is not the same as the energy

emitted or reflected from the same object observed from a short distance. This is due to the sun's azimuth and elevation and atmospheric conditions such as fog or aerosols, which influence the observed energy.

When an electromagnetic signal passes through the atmosphere, two processes affect the radiation: first, the absorption, which reduces its intensity, and second; the scattering, altering its direction. The first one happens when electromagnetic radiation interacts with gasses such as water vapor, carbon dioxide, and ozone. Hence radiometric distortions need a correction, to have the real reflection.

Radiometric correction removes the effects of atmospheric scattering and absorption, which occurs as the electromagnetic signal from the sun, passes through the atmosphere on its way to the target and from the target to the satellite (Du et al. 2002). Radiometric correction thus ensures that the results from the satellite image represent actual changes on the Earth's surface and are not due to differences in atmospheric conditions, or sensor calibrations.

Imagery can be radiometrically corrected to at-sensor radiance, at-sensor reflectance, or at ground reflectance. Radiometric corrections of optical images include 1) sensor radiometric calibration, 2) surface reflectance retrieval, 3) spectral characterization, and 4) georadiometric effects on image radiometry. Surface reflectance is caused by the scattering and absorption of the electromagnetic energy while passing through the atmosphere to the satellite sensor (Teillet et.al 2010). Since the optical features of the Earth's atmosphere are not identical spatially or temporally, corrections for these effects in the solar-reflective spectral bands are needed to fix satellite images.

Many researchers have studied the necessity of atmospheric correction when performing land cover change detection. Song et al. (2001) proposed that atmospheric correction may not be essential when using post-classification change detection under one condition; image scenes are classified separately with training data derived from the image to be classified. However, these researchers also found that atmospheric conditions could impact the results when image ratios were used. In contrary, Mahiny and Turner (2007) stated that atmospheric correction could influence the results of vegetation change detection and landscape metrics and hence, perform atmospheric correction can enhance accuracy despite different advantages and disadvantages.

Similar to geometric correction, radiometric correction is classified into two types; absolute and relative radiometric correction (Xie et al., 2008). Absolute radiometric correction attempts to measure or convert the surface reflectance of the target area using the sensor calibration data, the sun angle and view angle, and information about atmospheric conditions at the time and location of image acquisition (Du, Teillet, and Cihlar 2002). Relative radiometric correction adjusts (normalizes) radiometric measurements of one image toward a base or a selected reference data at a given moment. Several techniques exist for absolute radiometric correction, including ground reference, image-based, and atmospheric modeling techniques (Hadjimitsis et al. 2010).

Ground reference methods involve the collection of spectral data at specific ground locations at the time the satellite passes overhead. Scene data are adjusted based on the differences between scene values and collected values at specific locations. Dark object subtraction is a commonly used image-based technique which assumes image scenes contain features with zero or near-zero reflectance. Any deviations from zero in spectral values from these elements are supposed to be from atmospheric scattering and scenes are adjusted accordingly (Schroeder et al. 2006). A radiative transfer model uses information on atmospheric conditions at the time of sensor overpass to convert digital number data of the original scenes into at-ground spectral reflectance units. Atmospheric conditions for historical imagery are typically non-existent or are difficult to acquire in which case radiative transfer models apply standardized values based on latitude, season, aerosol measurements, and estimated surface temperature. An alternative, for historical imagery, is to use a relative radiometric correction (Small 2002). Several techniques exist for relative radiometric correction, including dark object subtraction, ridge method, and pseudo-invariant features.

 These techniques assume that there is a linear relationship of spectral values between two image scenes. Dark object subtraction can be used as a relative radiometric technique by selecting the darkest objects in a master scene and adjusting the other scene accordingly (Chen et al. 2005). In the ridge method, a density plot, comparing band to band, of two scenes is used to find a peak of solid values between the two scenes.

Regression coefficients are determined for each band by passing a line through the center of the density plots (Song et al. 2001). Pseudo-invariant features (PIFs), a mathematical model, and regression analysis are used to normalize one image (slave image) to a base (master image). This

technique assumes that there is a linear relationship between slave image pixels and master image pixels at the same image locations (Li et al., 2005).

To determine the linear relationship, spectral values of PIFs are collected from the master and slave images. PIFs are features which are spatially well defined and whose spectral reflectance properties have not changed or have changed tiny, over time (Song et al. 2001). PIFs represent the brightest and darkest features in an image and can be selected by various automated or manual methods. The set of spectral values is then inputted into a mathematical model, which is used to transform the slave image pixels to reflectance values normalized to the master image.

## 2.4.2 Calibration

Cross-calibration is the radiometric comparison of one sensor to another sensor on different satellites. Images are cross-calibrated if they are calibrated to a common source such as an integrating sphere before launch. Cross-calibration of space-based Earth observing systems is the way to guarantee consistency between two time series from two different sensors to build long-term time series of observations. There are several reasons that cross-calibration is needed (Giri, 2012); 1) While data from multiple sensors are increasingly employed to gain a more comprehensive understanding of land-surface, it remains challenging and costly to put sensors on an absolute radiometric scale, 2) Cross-calibration is the only viable solution to tie similar or different sensors onto a common radiometric scale while keeping consistency in quality, 3) It is most useful when onboard references are not available or vicarious calibrations are limited.

Cross-calibration is usually necessary following absolute radiometric correction because sensor calibrations may change or degrade over time causing differences in scenes, which are not due to actual changes on the ground nor atmospheric conditions (Yang et al. 2003; Coppin et al. 2004). Cross-calibration techniques are identical to related radiometric correction methods described in the previous section except that they are performed on scenes, which are corrected using the absolute method. In some studies, cross-calibration is replaced by relative radiometric correction as they state that relative radiometric correction can sufficiently account for the effects of atmosphere and sensor calibration (Furby and Campbell 2001).

Other studies, however, have shown that performing cross-calibration after absolute radiometric correction can produce more consistent image-to-image reflectance. Schroeder et al. (2006), in their search for the most useful radiometric technique for performing change detection, reported that consistent measurements of the surface reflectance for the same land cover over time (also referred to as common radiometric scale) were more useful for change detection than obtaining actual surface reflectance. This was because absolute correction techniques can in fact make the images less spectrally similar. Where vicarious calibration can be labor-intensive and limit the number of calibrations performs, cross-calibration can coordinate observations from different sensors, and facilitate a better approach to validate the absolute calibration accuracy.

## 2.4.3 Classification

Classification methods provide a system for assigning land cover on the ground to informational classes (Gao 2009). The scheme selected is ultimately determined by the land cover map needed; however, there are some general guidelines recommended for determining classes. Land cover classes should be mutually exclusive (land cover should belong to only one class), exhaustive (all classes in landscape accounted for), and hierarchical (specific categories can be collapsed into more general categories; (Congalton and Green 2009). Using a nationally or internationally recognized scheme offers the opportunity for other researchers to compare and contrast research results.

Frequent use of image classification have caused these aspects be automated; the researchers just need to provide certain input for the process of classification. Based on the amount of human interaction during classification, there are two types of approaches; supervised and unsupervised classification. Supervised classifiers are classifiers that by using a set of training data (Lu and Weng 2007) collected for each class are calibrated. This kind of classification requires the researcher select a proper classification scheme, and provide training sites within the image, with the best presentation of each class. A land cover classification system may include different classes, such as ground, water, forest, and building.

Each site that falls into a single class would have slightly different spectral characteristics, and enough number of training locations in each class must be provided by the analyst represent the

variation present within each class in the image. The classifier then uses spectral characteristics of the training sites to classify the remainder of the image. Supervised classifiers are easy to use and can give accurate thematic maps; however, they depend upon the quantity and quality of the training data (Foody and Mathur 2004). A proper supervised classification depends on the analyst's ability to provide sufficient numbers of training samples and to realize when training data can be transferred from one image to another (This topic is discussed further in the section "Training: Classifier Calibration").

On the other hand, unsupervised classification requires fewer numbers of inputs for the analyst during or before the processing. The classification algorithm automatically searches and analyzes the image, extracting clusters that are representative of the image content. The image analyst can check the post-classification results and determine if the extracted classes have to mean in the context of the image. This method has a few drawbacks; 1) to determine the meaning of each class identified by the unsupervised algorithm, 2) it requires a significant amount of time 2) to optimize the number of classes to initialize the algorithm, it also needs experimentations 3) there is no guarantee that the classes obtained in one image will be identical to the classes in the second image. Because of the above drawback, it may even take a longer time to interpret the unsupervised result than to conduct a supervised classification.

Classification schemes may be comprised of hard, discrete categories; hard classifiers assign each pixel to only one land cover class. Hard classifiers are popular because they are simple to use, they are computationally efficient, and they produce only one thematic map output layer. The supervised classifiers are some of the most commonly used of the many classifiers available, however as stated by Jensen (2005), there is not any distinguished classification method and the analyst himself can select the most appropriate method based on efficiency, effective time and cost relating to the area of study, source of data and the aim of research.

To have an unsupervised method of classifying for the images in this study, first, K-Means have been selected which states for calculating the initial class means, they are randomly distributed in the data space, then using a minimum distance technique (Anil, Z 2010) iteratively clusters the pixels into the nearest class, recalculate the related class means and reclassify the pixels by means of new means, this procedure will be iterated.

# 2.5 Principal Components Analysis (PCA)

A method in which a set of data is transformed into a new set of data with a better capture of the essential information is called principal components analysis (PCA). It converts an original set of data which are highly correlated into a substantially smaller set of uncorrelated data, which still contains most of the information from the original data set (Jensen 2005). Some variables are often highly correlated such that the most of the information represented by one variable is a copy of the information contained in another variable. PCA reduces or eliminates redundancy, which commonly exists in multiple Landsat bands, and condenses the information in inter-correlated variables into a fewer number of variables, are called principal components. This reduces processing time and allows classification algorithms to focus on spectral data, which contribute the most information to classification (Gao 2008).

In this method the original transformed data takes a new coordinate system, the number of output by the transformation is less than or equal to the number of input bands. If the original data contains a different number of variables, then each observation may be considered as a point in dimensional vector space. An interesting feature of the PCA transformation, particularly when it is applied to a set of data with several spectral bands, is that it extracts and concentrates almost all of the information in first the few components. The other components contain the same information in the main variables or the noise. Hence considering these components will reduce the volume of data greatly is to processed.

Some research indicates that first principal component has a strong association with brightness levels in an image, while the second principal component has a strong association with vegetation (Harris 2003). This is similar to the brightness and green output bands of TCT; however, it was difficult to determine the relationships of PCA components with brightness and vegetation with a visual inspection, and this may cause a misinterpretation (Coppin et al. 2004). Although finding the correlation of principal components to particular land cover is yet a complicated process, research has shown that PCA can be helpful in the detection of land cover in images with different registry date and time (Henry 2008).

# 2.6 Accuracy Assessment: Reference Data and Reporting

In the field of image analysis and information processing, there are two terms; accuracy and precision. Accuracy evaluates the correlation between a standard that is assumed to be correct and a classified image that is of unknown quality. Precision refers to some details that are found in the classification. To increase the accuracy, it is possible to decrease the level of detailed information in the classification or to pick more general classes rather than very specific ones. For instance, a scheme that classifies trees vs. crops provides less chance for classification error than one that recognizes many different types of trees and different kinds of vegetables. In this example, lower precision presents the potential for higher classification accuracy. However, the analyst of the image that selects only general classes cannot make accurate statements about any given point on the image.

Classification error occurs when a pixel of an image (or a feature) that belongs to one class is assigned to another class. There are two types of errors; an error of omission and error of commission. The error of omission refers to an error that happens when a feature is left out of the class that is being evaluated, whereas error of commission indicates the error that occurs when a feature is incorrectly included in the class that is being evaluated. An error of omission in one class can associate to an error in commission in another class.

Comparison between the map created by remote sensing and reference map which is based on the different information source can lead to an acceptable accuracy. One of primary purposes of accuracy assessment and error analysis is quantitative comparisons of different interpretations which leads to an acceptable precision, and answers the question why the remote sensing analysis is needed if the reference map is already existed by using a pixel-by-pixel, point-by-point comparison, different procedures of classification, by different individuals, or from images acquired at different times, can be achieved. Although, in the application, we have to determine which one is the most useful or the most correct one.

Most often, the accuracy of image classification is reported as a percentage of correct results. By using the consumer's accuracy takes errors of the commission into account, by telling the user that, for all areas identified as a category, a certain percentage are actually correct. The ratio of correctly

classified pixels to the pixels assigned to a particular group is called consumer's accuracy. Another ratio is called Producer's accuracy, which measures the accuracy of classified maps.

To assess the accuracy of classified maps, land cover on the map should be compared to actual land cover on the ground. The confusion matrix, by far the most commonly used technique, compares a set of ground reference data to the classified map. The confusion matrix gives a measure of the overall accuracy, (i.e., total number of correctly classified samples), producer's accuracy (i.e., measure of omission; probability that a ground reference test sample is classified properly in the map), and user's accuracy (i.e., ratio of commission; probability that a sample from a map actually represents that category on the ground; Congalton 1991).

It also provides a Kappa coefficient of agreement (Congalton 1991) that accounts for chance agreement in the overall accuracy value, even though Pontius and Millones (2011) have recently shown its limitations. Finally, the McNemar test is useful for determining if differences in classification accuracies obtained by different classification approaches are statistically significant (Debeir et al. 2002; De Leeuw et al. 2006 (Foody and Mathur 2004). The null hypothesis of the McNemar test is that map accuracy (proportion of correctly classified pixels) is the same regardless of which classification algorithm is used (De Leeuw et al. 2006). If the McNemar test results in a value higher than 3.84, the null hypothesis is rejected and map accuracies are considered significantly different (statistically) with a 95 percent degree of confidence. The confusion matrix and McNemar test require reference data as input. Reference data should be collected using a stratified disproportionate random sampling scheme (Stehman and Czaplewski 1998) for the same reasons noted for the training data above. It is important that unbiased reference data are used in evaluating classified map accuracy and that data collected for training are not also used for testing (Congalton and Green 2009; Stehman and Czaplewski 1998). As with training data discussed above, sampling scheme, sample size, and data collection methods are critical in the context of the data used for assessing the accuracy of the classified maps.

# Chapter 3

# Monitoring and evaluation of the urban reconstruction process in Bam

# 3.1 Introduction

The city of Bam is located in Kerman Province in southeastern Iran, at a distance of 980 km from the capital city, Tehran (see Fig. 3.1a). On December 26, 2003, a devastating earthquake with a $M_w$ of 6.6 struck the region, severely damaging the city. Although it lasted for just a few seconds, more than 22,000 lives were lost (Eshghi et al. 2004), and 80% of the city's buildings were completely destroyed (Nadim et al. 2004). This earthquake damaged almost all of the city's brick and adobe buildings, including the famous "Arg-e Bam" (Bam Citadel), which was over 2,000 years old and was listed as a component of the "Bam and its Cultural Landscape" World Heritage Site in July 2004. The city's municipal facilities and infrastructure were also destroyed. While a study showed that destructive earthquakes of a similar magnitude had previously struck the province over a time span of 2,000 years, Bam itself has never before experienced a significant event such as this one (Allamezadeh et al. 2005).
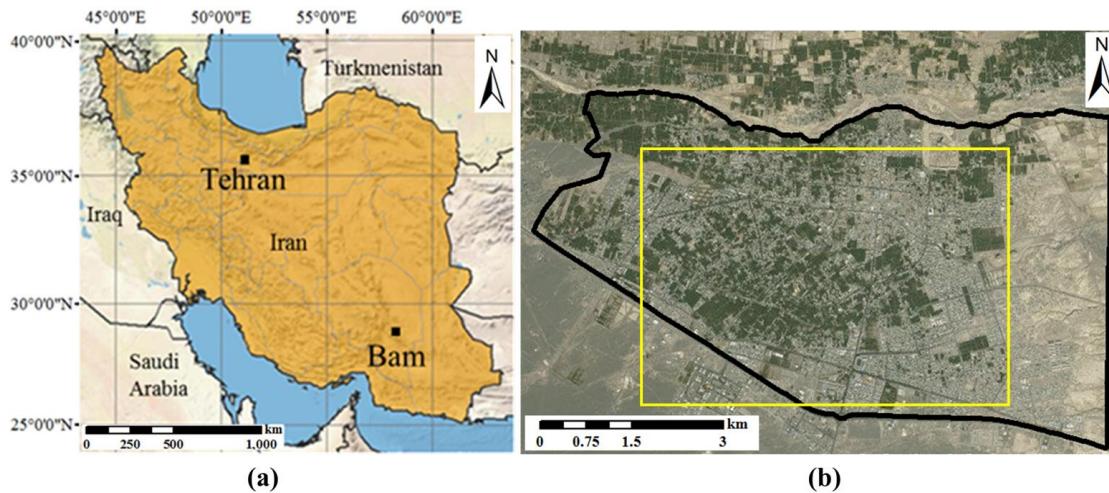


**Fig. 3.1** (a) Location of Bam, Iran, (b) Bam city border (black line) and the region of interest analyzed in this study (the yellow rectangle).

Soon after the occurrence of the earthquake, a large number of studies were carried out to assess the impact of the earthquake and the degree of damage that it caused (Chiroiu 2005; Yamazaki et al. 2005; Gusella et al. 2005; Kohiyama and Yamazaki 2005; Rathje et al. 2005). Several studies have been conducted to evaluate the effect of public participation during the reconstruction phase implemented after the disaster and to identify key players during this phase (Omidvar et al. 2011). Ghafory-Ashtiany and Hosseini (2007) have discussed rescue and relief operations and the

replacement of buildings and infrastructure based on the results of field surveys and official statistics. Kitamoto et al. (2011) have also carefully monitored the reconstruction of the Bam Citadel as one of notable World Heritage Sites that was destroyed by the earthquake. This study encompassed the techniques applied and policy decisions. However, no study has so far been conducted to assess renovation and reconstruction of the city over the decade following the Bam earthquake. Moreover, none of the previous studies have used satellite images and remote sensing technologies to monitor the progress of the reconstruction work.

In general, the process of reconstruction is an important component of disaster management. It demonstrates the efforts made by a government to alleviate hardships experienced by the affected population after a disaster and its ability to satisfy the needs of survivors (Murao et al. 2013). Therefore, investigating and understanding the reconstruction process is a useful method for evaluating the performance of the implementers of reconstruction. However, official statistical data are not always the best data source, because this information is partially collected by the same institute that is responsible for the project's execution. By contrast, the assessment of satellite images provides a direct, objective, independent, and more reliable method of evaluating reconstruction projects.
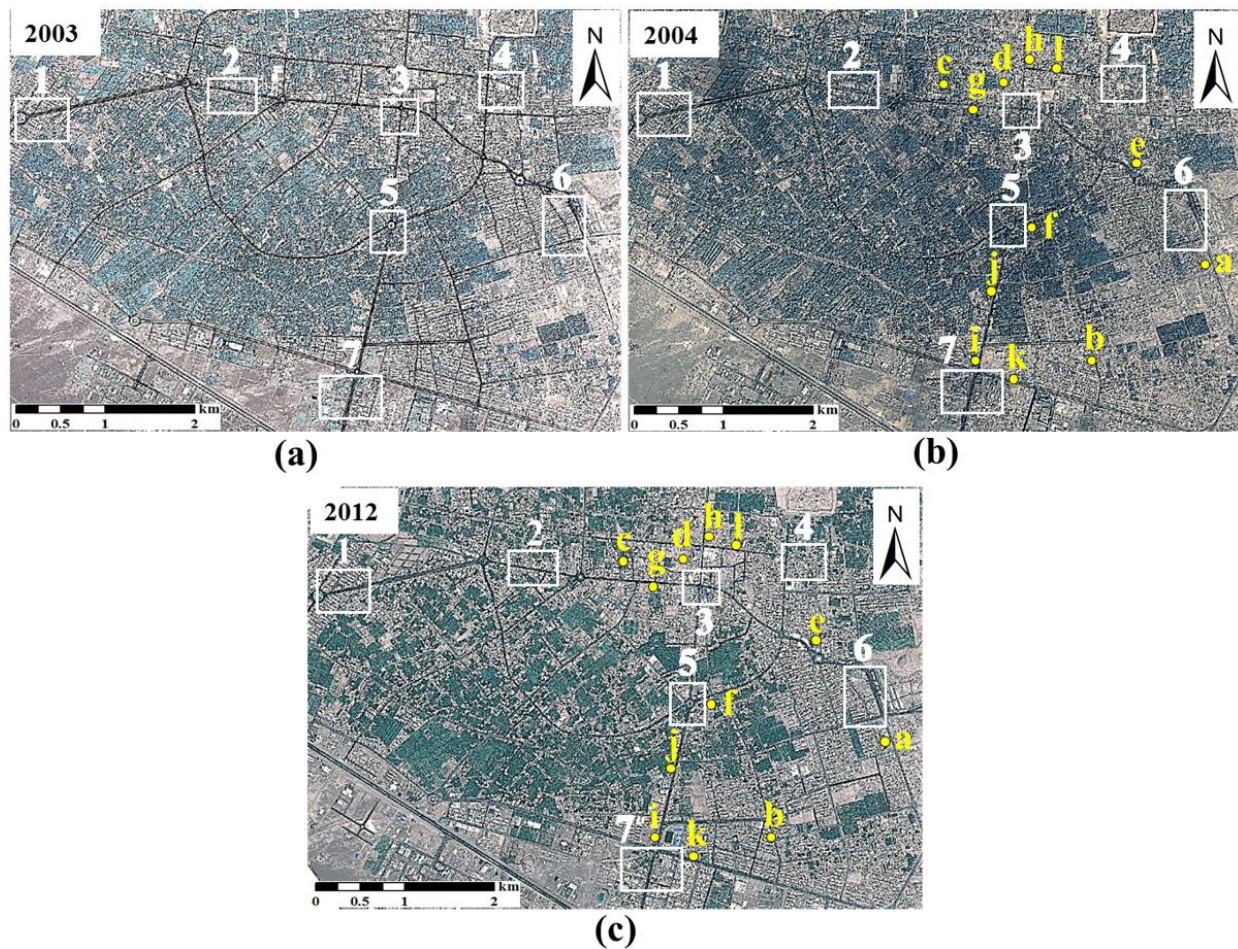
**Fig. 3.2** (a) QuickBird image of Bam acquired on September 30, 2003, (b) QuickBird image acquired on January 3, 2004 (c) GeoEye-1 image acquired on August 11, 2012.

The yellow points represent the locations of sites observed in the field survey in 2004 and 2014. White rectangles represent the locations of the seven study areas.

For this study, we used different methods, including remote sensing, to evaluate the renovation and reconstruction process Bam over the decade following the earthquake. We examined the city's current status, including its residential buildings, public facilities, and other kinds of infrastructure using official statistical data, field survey data, and high-resolution satellite images to monitor its reconstruction. This study is the first of its kind to be conducted on Bam.

The study's methodology comprised four main components. First, official statistics and reports provided by the authorities were examined. These included the extent of the damage to buildings and the number of buildings, according to their structural type, before and after the earthquake. Second, we conducted field surveys of the reconstruction process based on photographs taken at the same locations at three different times after the earthquake. This enabled us to compare landscape changes and, especially, to observe changes in the physical environment. Third, we analyzed three satellite images of areas of the city captured before, immediately after, and eight years after the earthquake to identify any significant changes in buildings, land use, roads, and vegetation in two targeted study areas. In addition, we evaluated post-reconstruction changes relating to 632 individual buildings in the seven study areas. Last, we analyzed the data obtained for the three main components of the study, described above. Accordingly, we present a discussion of the overall reconstruction process in Bam.

## 3.2 Assessment of reconstruction

### 3.2.1 Assessment of reconstruction based on statistical data

We compiled and examined statistical data provided by the Bam Statistical Survey Center that is overseen by the Statistical Center of Iran (2004) as well as the official reports of the Islamic Revolutionary Housing Foundation (ISF), which is the principal executing agency responsible for Bam's reconstruction. Tables 3.1 and 3.2, respectively, provide statistics on Bam's population during different periods, and the degree of damage inflicted on the city's buildings.

**Table 3.1** Population of Bam at three different times (Statistical Center of Iran 2011)

| Year | 1996 | 2006 | 2011 |
|---|---|---|---|
| **Population** | **83,936** | **96,740** | **107,131** |

**Table 3.2** Effect of the 2003 earthquake on buildings (Statistical Center of Iran 2004)

| Before EQ | Immediately after EQ in 2004 | | |
|---|---|---|---|
| 28,625 | Destroyed | Partially Damaged | Intact |
| | **26,111** | **2,381** | **133** |

According to information available in the records of the Civil Engineering Organization of Bam, 33,126 construction permits have been issued. Of these, 26,540 were executed between early 2004 (following the earthquake) and March 2014. During this period, the Statistical Center of Iran (2011) also noted the existence of 26,708 residential units. This large number of units indicates the extent of reconstruction efforts and the scale of the budget allocated for this project. The Civil Engineering Organization of Bam has claimed that it has been monitoring the construction process. Consequently, these new structures would be expected to present a higher degree of resistance to an earthquake of a similar magnitude to the previous one.
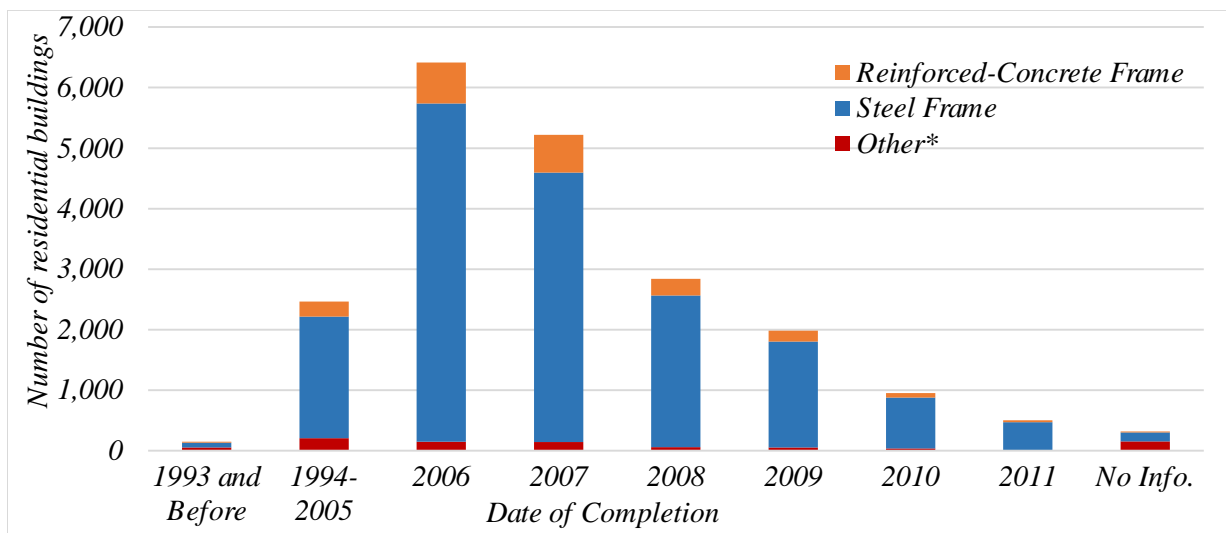


*Adobe, mud, clay, wood, cement blocks, brick

**Fig. 3.3** Number of residential buildings, categorized by the completion year and structural type

Figure 3.3 shows the number of residential units built during different periods and classified according to the materials used for construction. This figure reveals that more than half of the existing residential units in Bam in 2011 were completed in 2006 and 2007 (2–3 years after the occurrence of the earthquake). As of May 2006, 20,119 buildings were under reconstruction, and 7,206 residential buildings and 72 commercial buildings had been completed. In 2007 (3 years after the earthquake), the pace of reconstruction had evidently slowed down. In addition, we found that 12.5 % of the residential buildings were completed before 2005. Therefore, 87.5 % of these types of structures were newly constructed. Furthermore, 85.7 % of the city's residential buildings were found to have a steel structure, whereas 10.2 % were made of reinforced concrete, both of

which are usually selected by professional engineers and technicians working under the supervision of engineering institutions. Only 4.1 % of the existing residential buildings in 2011 were built using conventional and inappropriate frameless methods entailing the use of materials such as mud, clay, brick, and cement blocks that are not earthquake resistant. By contrast, prior to the earthquake, 69.0 % of such buildings were built using brick, wood, or clay (Ghafory-Ashtiany and Hosseini 2007).

## 3.2.2 Assessment of reconstruction based on field surveys

The first author carried out a field survey of Bam during visits to the area in March and September 2014. The selection of locations to be photographed was based on original sets of field photographs that were previously taken in different areas of Bam, with geographical coordinates assigned to most of these. These original sets consisted of around 2,000 photographs, which were taken by three different research groups 2, 4, and six weeks after the disaster in early 2004. Subsequently, in 2007, the second author took an additional 400 photographs of the city. Aligned with this archive, the first author prepared 1,500 photographs that mostly matched the previous photos using a GPS device.

The initial distribution of the damage was also considered in stratifying the selection of sampled sites. Several studies assessing the extent of damage in different parts of the city (Chiroiu 2005; Yamazaki et al. 2005; Gusella et al. 2005; Kohiyama and Yamazaki 2005; Rathje et al. 2005) have indicated that highly damaged structures were located in the center and in areas located east and southeast of the city. In addition, these areas of the city included key urban infrastructure and buildings such as banks, fire stations, and administrative offices. Therefore, more attention was paid to these strongly affected areas during the field surveys and photograph sampling (Fig. 3.2 b, c).

The field survey conducted in 2014 revealed four main findings, as follows.

• Abandoned buildings and bare lands: Abandoned buildings, most of which were severely damaged by the earthquake, could still be seen in some areas (see Fig. 3.4 [a and b]). In some areas, especially in the central and northern parts of the city that were severely damaged, all of the debris

had been removed, but the land remained bare in the absence of any reconstruction (Fig. 3.4 [c and d]).

• Repaired buildings: Some slightly damaged buildings had been partially renovated and were being used in that condition (Fig. 3.4 [e and f]).

• Public buildings: Almost all of the important public buildings—that is, mosques, banks, and governmental offices—had been reconstructed (Fig. 3.4 [g and h]).

• New buildings: New buildings had been constructed in the city, mainly in the eastern and southeastern parts, which, prior to the earthquake, had not been developed. These buildings included sports stadiums, a medical university, a commercial/administrative complex, a library, a cultural center, and a new residential district. Photographs of some of these buildings are depicted in Fig. 3.4 (i–l).
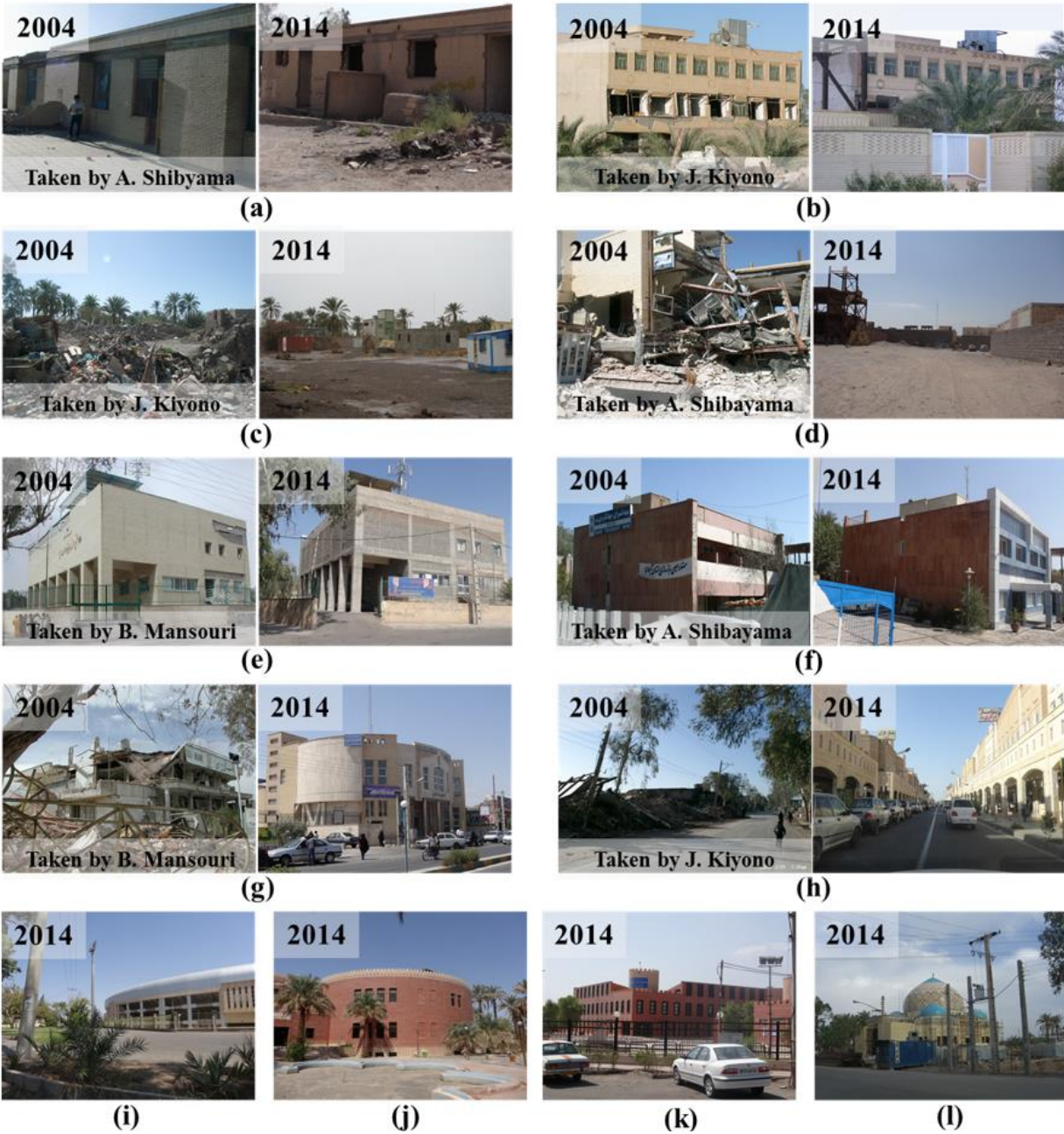
**Fig. 3.4** Photos of the same locations observed in the field surveys in 2004 and 2014: (a) & (b) abandoned buildings, (c) & (d) bare lands, (e) & (f) repaired buildings, and (g) & (h) reconstructed public places. Examples of new buildings in 2014, (i) Bam football stadium, (j) Bam central library, (k) Medical University of Bam, (l) Asiri mosque. The location of each site is displayed in Fig. 3.1d.

### 3.2.3 Assessment of reconstruction based on satellite images

We compared three high-resolution optical images of Bam that were captured by the QuickBird satellite on September 30, 2003 (Fig. 3.2a) and January 3, 2004 (Fig. 3.2b), and by the GeoEye-1 satellite on August 11, 2012 (Fig. 3.2c). Figure 3.1b shows the city's borders and the focal areas targeted for our analysis. For this study, we selected seven areas (see Fig. 3.2 [a–c]), based on a previous study by Hisada et al. (2004). These authors evaluated damaged buildings using the EMS-98 criteria (Günthal ed. 1998) and classified them into five groups according to the damage grade, ranging in severity from the least severe (G1) to the most severe (G5). Areas 1, 5, and 7, which are located in the western section, the city center, and the southern section, respectively, experienced relatively little damage. Areas 2, 3, and 4, which are in the northern section and Area 6, which is located in the western section of the city, were significantly damaged. We selected areas 1 and 3 to estimate land cover changes. All seven areas were analyzed to estimate changes in the buildings as a result of reconstruction.

## 3.3 Estimation of changes in land cover

We compared the satellite images of the slightly damaged area (Area 1) and the severely damaged area (Area 3) captured before the earthquake (2003) and eight years after the earthquake (2012) to detect changes in four main categories of urban land cover. These were: buildings, vegetation, roads, and ground. We used manual means of classification to detect land cover, namely, monitoring and comparing each component type of land cover. Our use of very high resolution (0.5 m) images enabled careful and accurate detection of land cover changes. Even though this method was very time consuming, we were able to distinguish old from new buildings. Figures 3.5 and 3.6, respectively, depict examples of unchanged and reconstructed buildings.
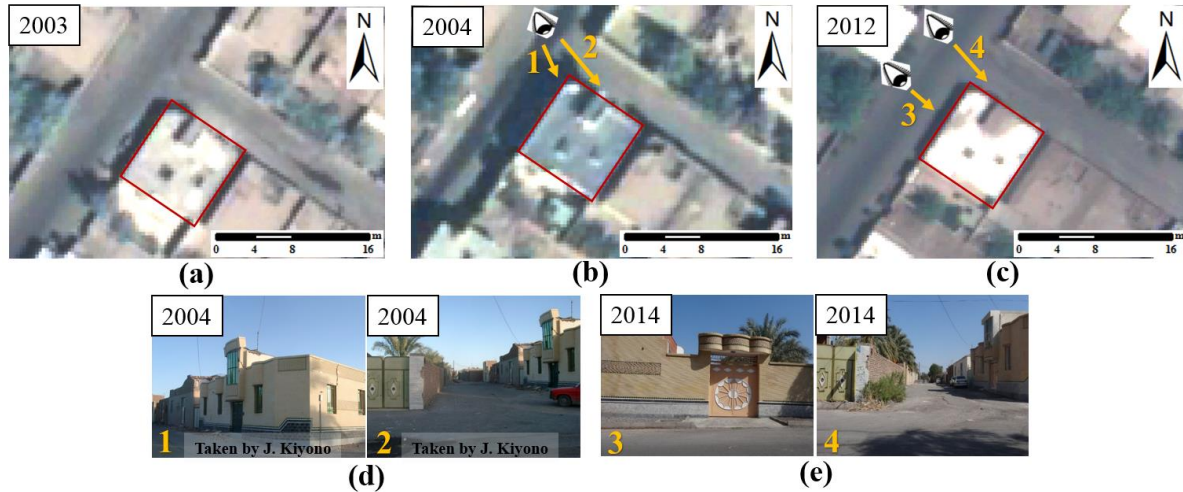
**Fig. 3.5** An example of unchanged building (Old building remains the same): (a) the building in 2003, (b) the building in 2004, (c) the building in 2012, (d) and (e) photos of the same building, collected in the field surveys of 2004 and 2014
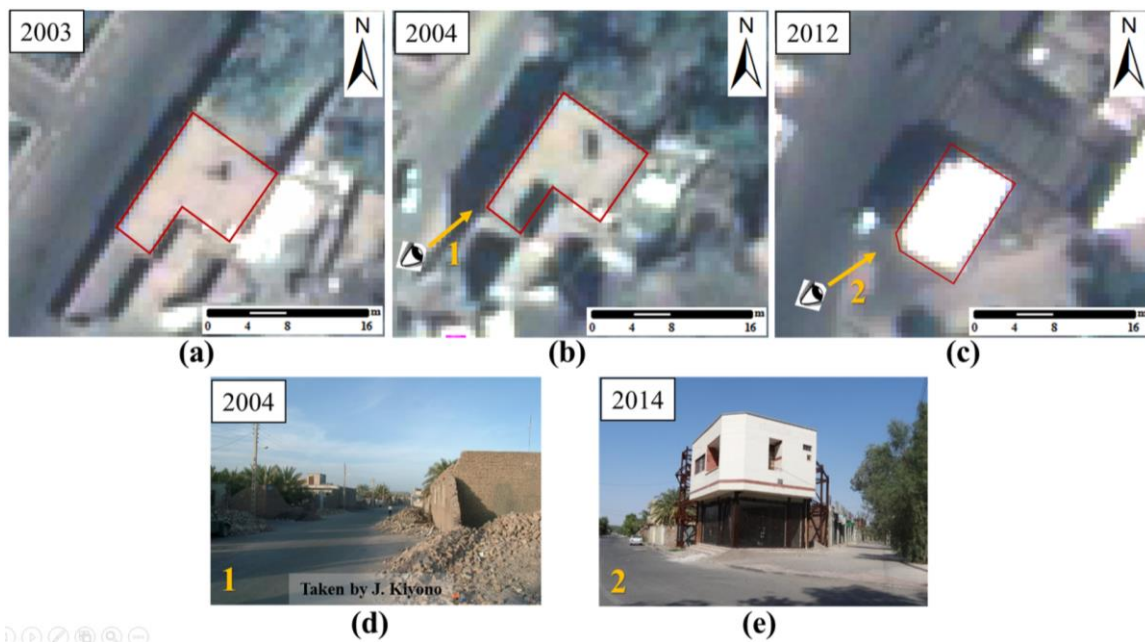


**Fig. 3.6** An example of a reconstructed building. (Old building changed to New building): (a) the building in 2003, (b) the building in 2004 (severely damaged), (c) the reconstructed building in 2012 in the same location, (d) photo of the destroyed and (e) reconstructed building, collected in the field surveys of 2004 and 2014

Figure 3.7 (a and c) shows satellite imagery of Area 1, with the manually classified land cover in 2003 and 2012, respectively. Yamazaki et al. (2005) found that this area was partially damaged,

as shown in Fig. 3.7b. Figure 3.8a lists the area-wise percentages of the four land cover categories (buildings, vegetation, roads, and ground). The image for 2012 reveals an increase in building-covered land and a decrease in ground covered land. Similarly, Fig. 3.9 (a and c) shows the land cover of Area 3 in 2003 and 2012, respectively. Figure 3.8b lists the corresponding area-wise percentages for the four land cover categories in this area. As observed by Yamazaki et al. (2005), and shown in Fig. 3.9b, this area was completely destroyed by the earthquake. Here, land covered by buildings and vegetation had decreased, whereas ground cover had increased significantly. A large tract of empty land was observed in the area, which implied the slow pace of the reconstruction process. Although the debris has been removed and the land has been re-zoned, reconstruction has not yet begun in this area.
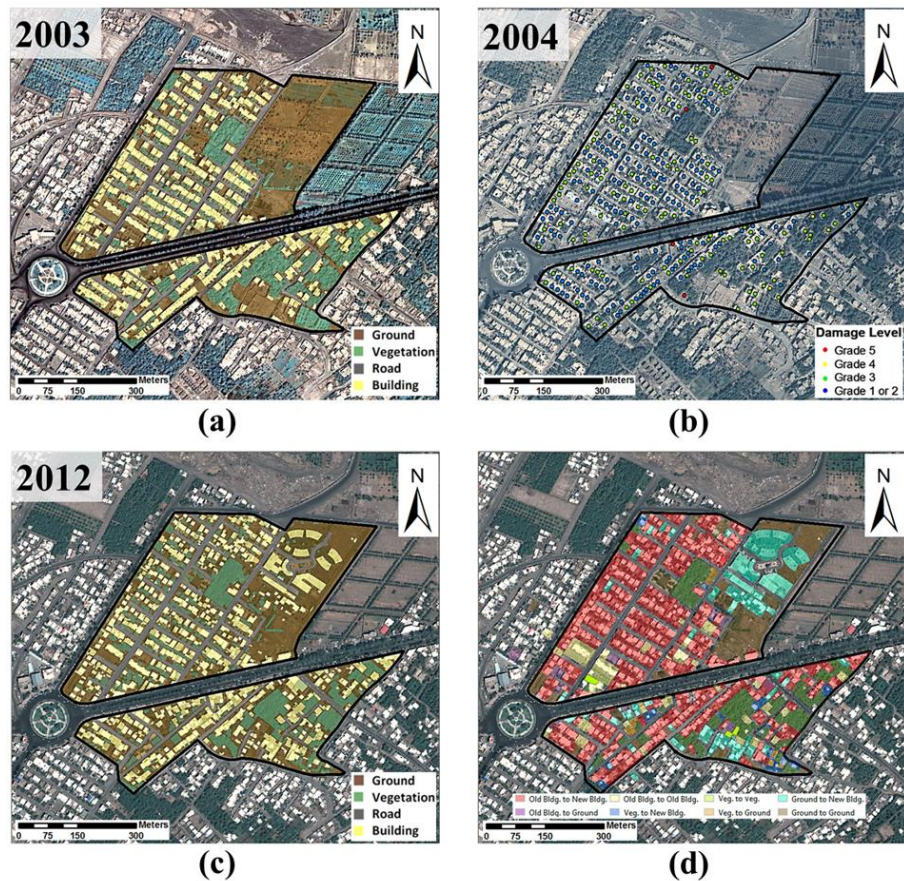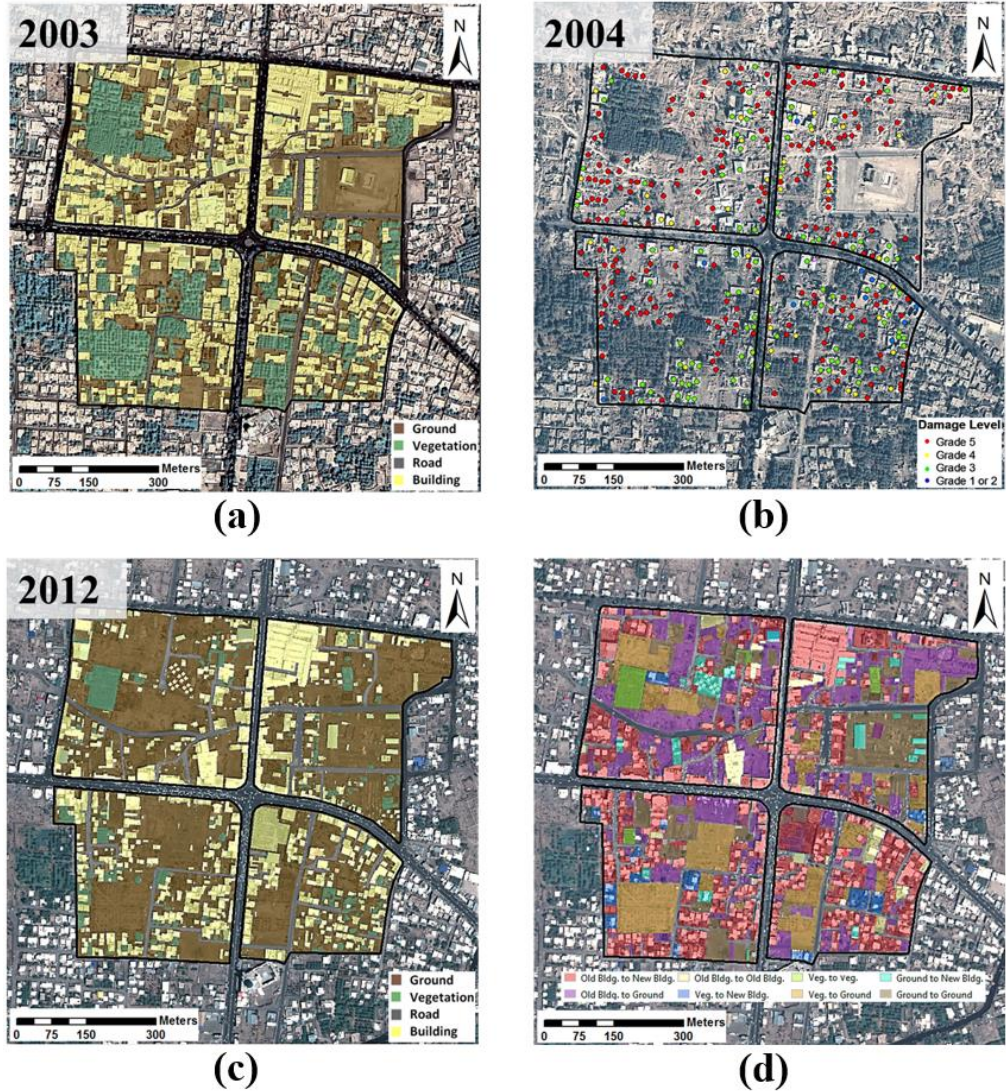


**Fig. 3.7** Analysis of Area 1: (a) manual classification of land covers in 2003; (b) damage level of individual buildings in 2004 (Yamazaki et al. 2005); (c) manual classification of land covers in 2012; (d) land cover changes between 2003 and 2012.
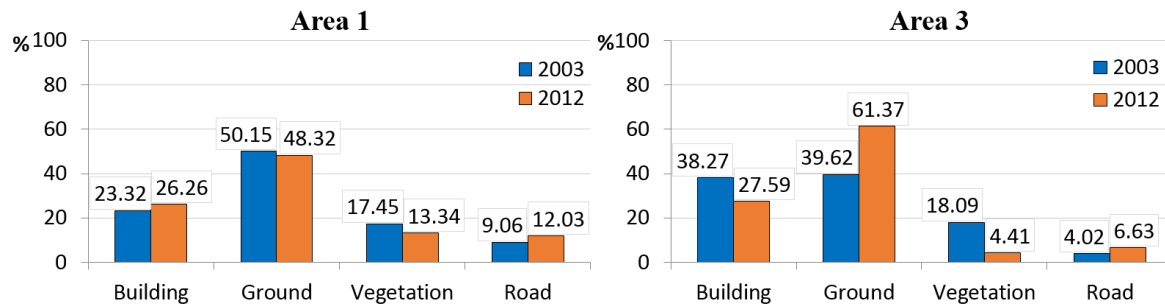
**Fig. 3.8** Percentages of land covers, *buildings*, *roads*, *vegetation* and *ground* in Area 1 (left) and Area 3 (right) in 2003 and 2012

As shown in Figs. 3.7d and 3.9d, respectively, land cover changes before and after the earthquake were classified according to ten different categories. These were "old building to new building," "old building, no change" (existed before 2003), "old building to vegetation," "old building to ground," "vegetation to new building," "vegetation, no change" (existed before 2003), "vegetation to ground," "ground to new building," "ground to vegetation," and "ground, no change" (existed before 2003). Table 3 lists the area-wise percentages of these land cover changes.

**Fig. 3.9** Analysis of Area 3: (a) manual classification of land covers in 2003; (b) damage level of individual buildings in 2004 (Yamazaki et al. 2005); (c) manual classification of land covers in 2012; (d) land cover changes between 2003 and 2012

**Table 3.3** Land cover changes (in percent) from 2003 to 2012

(a) Area 1

| 2003 \ 2012 | New Building | Old Building | Vegetation | Ground | Total |
|---|---|---|---|---|---|
| Old Building | 50.9 | 6.7 | 0.0 | 1.7 | 59.3 |
| Vegetation | 2.2 | - | 10.8 | 1.1 | 14.1 |
| Ground | 13.0 | - | 0.3 | 13.3 | 26.6 |
| **Total** | **66.1** | **6.7** | **11.1** | **16.1** | **100.0** |

(b) Area 3

| 2003 \ 2012 | New Building | Old Building | Vegetation | Ground | Total |
|---|---|---|---|---|---|
| Old Building | 39.5 | 2.9 | 0.0 | 22.5 | 64.9 |
| Vegetation | 3.3 | - | 2.0 | 14.0 | 19.3 |
| Ground | 3.2 | - | 0.0 | 12.6 | 15.8 |
| **Total** | **46.0** | **2.9** | **2.0** | **49.1** | **100.0** |

From Fig. 3.7d, we can observe that in Area 1, which was partially damaged, the majority of land covered by old buildings and part of the ground changed to new buildings. This finding was contrary to our expectation and will be subsequently discussed. In contrast, Fig. 3.9d shows that in Area 3, which was extensively damaged, the majority of old buildings and vegetation changed to ground cover. This observation is consistent with the slow recovery of severely affected areas that has been widely observed, worldwide, in zones hard hit by natural disasters (JICA, 2013).

# 3.4 Estimation of changes in the buildings

In this section, we consider reconstruction from a different perspective. Based on the previously mentioned study by Hisada et al. (2004), who assessed and categorized the damage grades of buildings according to the five classes of EMS-98 (G1 to G5), we selected 632 buildings in the

same seven study areas. Using satellite images, along with the results of our field investigations, we evaluated changes that had occurred in existing buildings (in 2003) from the time of the earthquake up to August 2012. We delineated three groups based on the kinds of building changes.

•        No change: Buildings that existed before the earthquake and were still standing in 2012 without evidencing any change, or just minor repairs, or that had been abandoned.

•        Changed and renewed: Buildings existing in 2012 that had been completely rebuilt after the earthquake.

•        Vacant land: Buildings that existed before the earthquake that had changed to bare land in 2012.

Figures 3.10 and 3.11 show the damage grade and the type of change for individual buildings in all seven study areas. Table 4 shows the number of buildings and the type of change in each study area, based on the damage incurred and current status. According to the study by Hisada et al. (2004), the apportioning of buildings by damage grade was as follows: G1 (19 buildings), G2 (110 buildings), G3 (122 buildings), G4 (104 buildings), and G5 (277 buildings) across the seven study areas. This indicates that 61 % of all buildings belonged to the G4 and G5 categories, and were severely damaged or had collapsed as a result of the earthquake. Only 20 % of buildings in the seven study areas survived with slight or minor damage (G1 or G2).
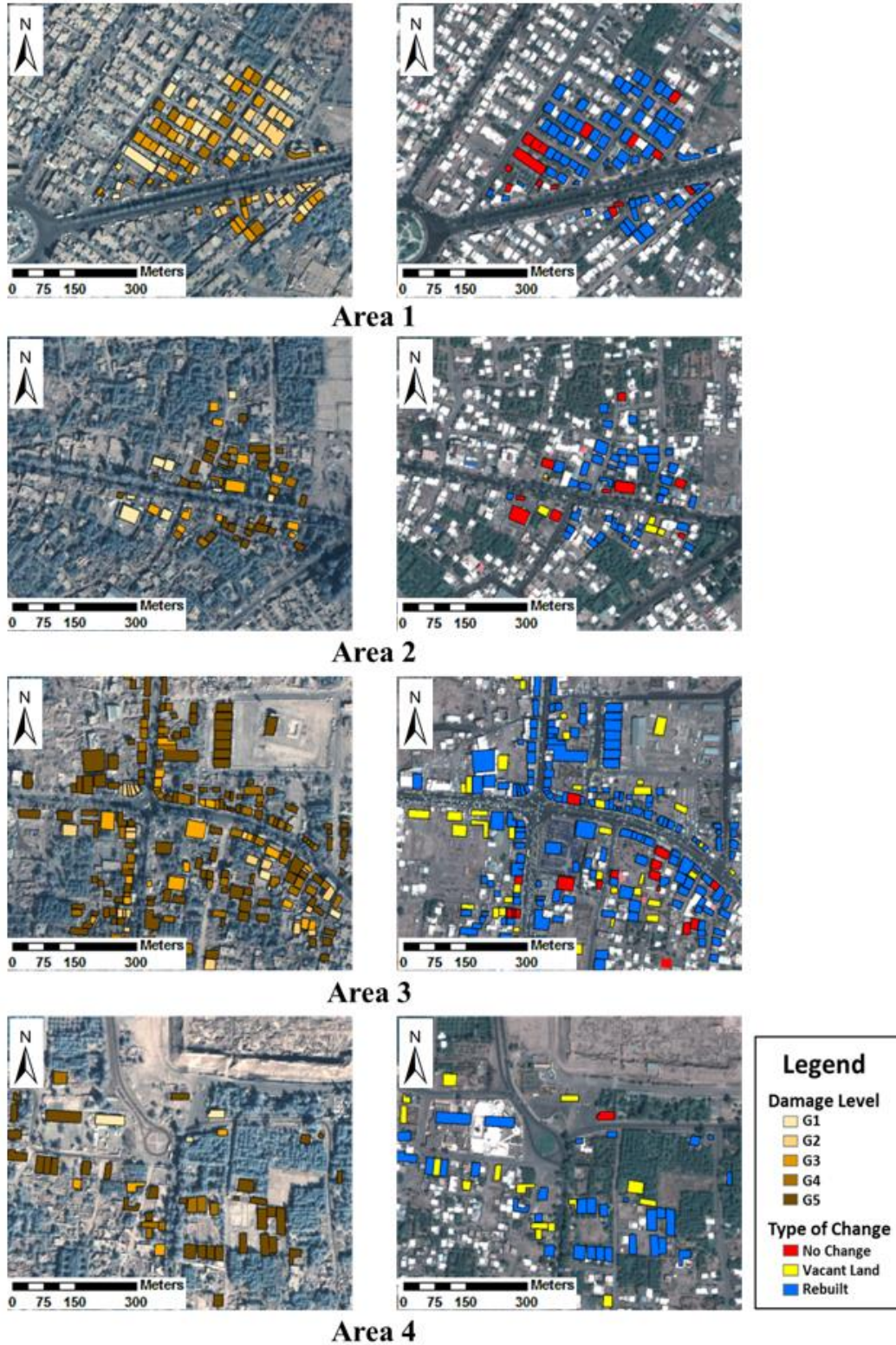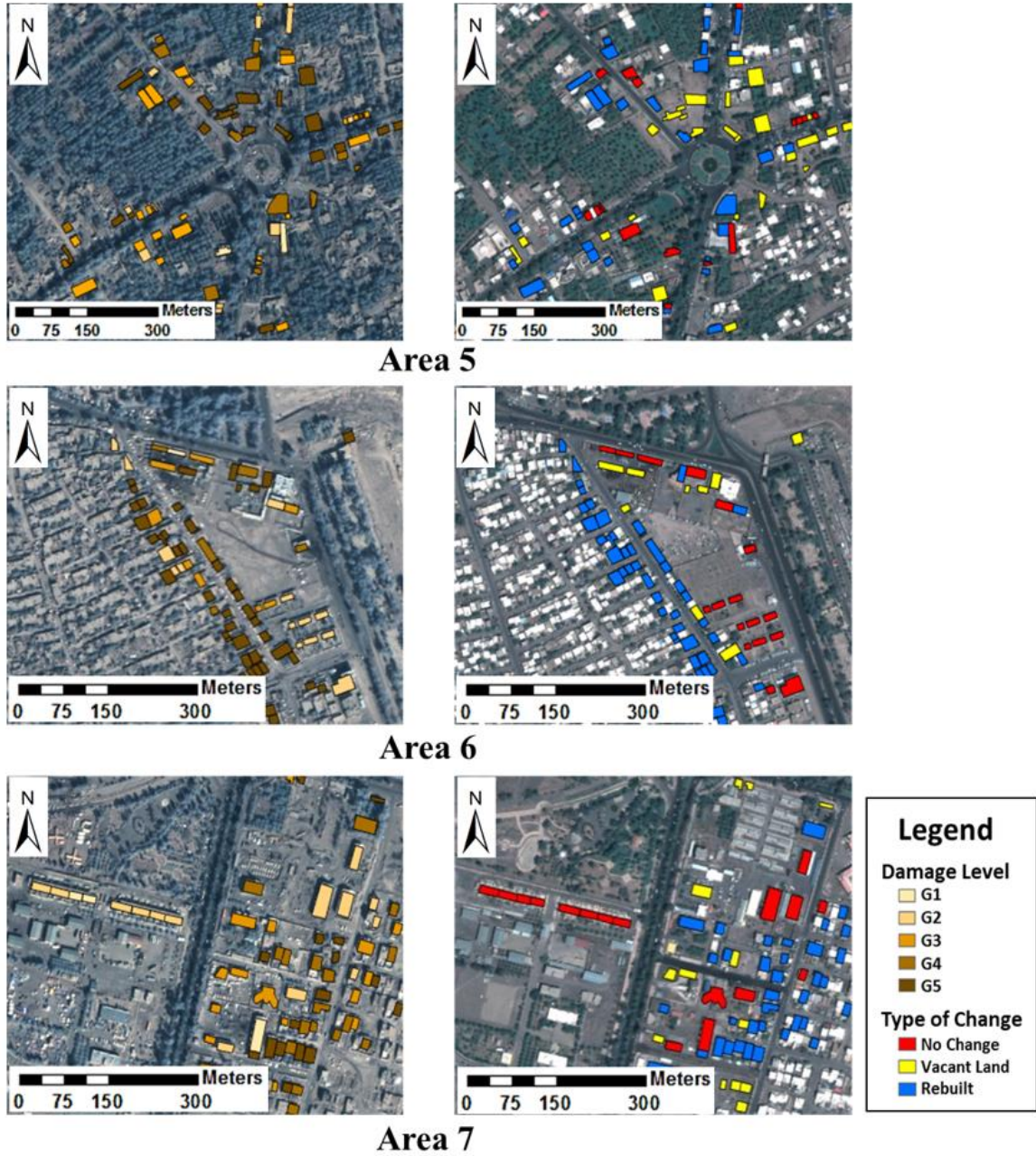
**Fig. 3.10** Damage level (left) and the type of change (right) for each individual building in Areas 1, 2, 3

**Fig. 3.11** Damage level (left) and the type of change (right) for each individual building in Areas 5, 6 and

Of the 632 buildings, in total, 421 were reconstructed between 2003 and 2012. In 2012, 100 were found to be unchanged, and 111 had changed to vacant land. Of the 129 buildings categorized as G1 and G2, 66 had been reconstructed, while 61 remained unchanged. Of the 381 G4 and G5 buildings, 282 had been reconstructed while 13 remained unchanged. Only two G1 and G2

**Table 3.4** Number of buildings in each study area based on the damage level and the type of change

| Damage Level | G1 | | | G2 | | | G3 | | | G4 | | | G5 | | | Number of Buildings |
|---|---|---|---|---|---|---|---|---|---|---|---|---|---|---|---|---|
| Type of Change | N | V | R | N | V | R | N | V | R | N | V | R | N | V | R | |
| Area 1 | 4 | 0 | 6 | 7 | 0 | 28 | 5 | 0 | 22 | 0 | 0 | 13 | 0 | 0 | 3 | 88 |
| Area 2 | 0 | 0 | 0 | 6 | 0 | 2 | 2 | 1 | 8 | 1 | 0 | 6 | 0 | 4 | 23 | 53 |
| Area 3 | 2 | 0 | 1 | 7 | 2 | 12 | 5 | 1 | 15 | 6 | 4 | 31 | 1 | 31 | 93 | 211 |
| Area 4 | 0 | 0 | 0 | 1 | 0 | 2 | 0 | 4 | 3 | 0 | 2 | 2 | 0 | 10 | 26 | 50 |
| Area 5 | 2 | 0 | 0 | 6 | 0 | 9 | 10 | 10 | 10 | 1 | 4 | 10 | 0 | 15 | 12 | 89 |
| Area 6 | 1 | 0 | 0 | 9 | 0 | 5 | 3 | 1 | 4 | 3 | 0 | 2 | 1 | 8 | 34 | 71 |
| Area 7 | 3 | 0 | 0 | 13 | 0 | 1 | 1 | 6 | 11 | 0 | 4 | 15 | 0 | 4 | 12 | 70 |
| Total | 12 | 0 | 7 | 49 | 2 | 59 | 26 | 23 | 73 | 11 | 14 | 79 | 2 | 72 | 203 | |
| Number of Buildings | 19 | | | 110 | | | 122 | | | 104 | | | 277 | | | 632 |

**N**: No change between the earthquake and 2012
**V**: Vacant land, no rebuilding in the location after the destruction of the existing building
**R**: Buildings were rebuilt or renewed between 2003 and 2012

buildings had changed to vacant land, whereas 86 G4 and G5 buildings had been abandoned and demolished, leaving empty land in their place.

Our comparison of these land use changes, categorized into three classes (no change, rebuilt, and vacant), and the number of buildings categorized into five classes according to their level of damage (G1 to G5), revealed a correlation between the level of damage and the reconstruction process. This comparison suggested an increase in the ratio of reconstructed buildings and the areas of vacant land in proportion to the level of damage of the buildings, as shown in Fig. 3.12. Similarly, the number of unchanged buildings was higher in slightly damaged areas.
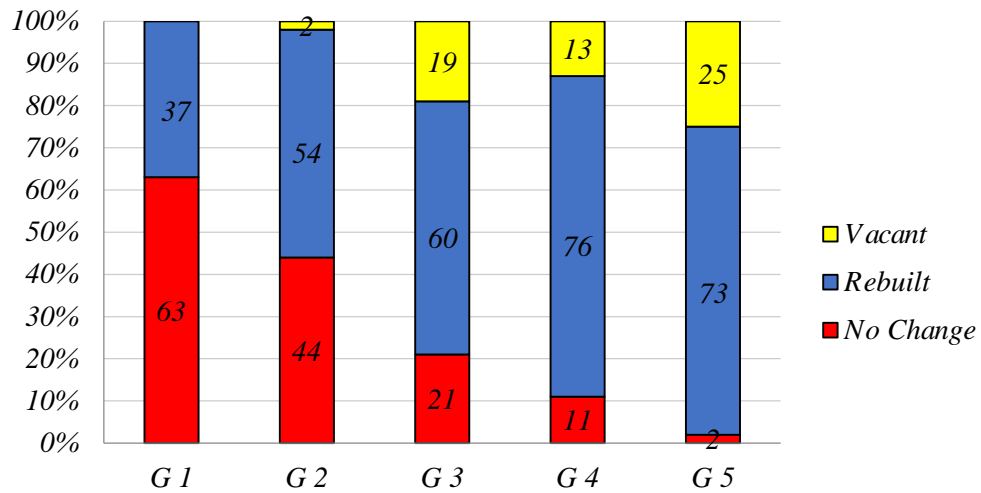
**Fig. 3.12** Percentages of the types of change for buildings with different damage levels (G1–G5)

## 3.5 Results and discussion

Several major findings that were consistent with the field survey results emerged from our evaluation using satellite images to determine land cover changes, as discussed in section 4.1. First, most of the reconstruction of damaged structures occurred in the same location. Moreover, some of the buildings that had not been seriously damaged, particularly those in Area 1, were completely renovated. In addition, new buildings (e.g., gyms and commercial complexes) were constructed on previously empty lots, thus indicating an increase in the use of new land for construction in the area. In the center of the city, vegetation and green spaces were destroyed and changed to bare land.

Further, a comparison of land cover changes with statistical data showed that although there is still a considerable area of vacant land in the central and northern parts of the city, a sufficient number of housing units have been constructed. This can be attributed to the increase in the number of units and the population density in the reconstructed areas. Most of the former buildings consisted of just one or two family units. However, the reconstruction has resulted in new buildings with more floors and family units. Therefore, the total number of units exceeds that prior to the earthquake, even though the amount of empty land has also increased.

A current issue that affects the city is the transformation of a considerable proportion of land with vegetation into empty ground after the earthquake. There are two main reasons for this phenomenon. The first is the destruction of networks of Qantas (aqueducts) (Statistical Center of Iran 2004), which provided the main source of irrigation in the dry desert environment of Bam. The second reason is the high rate of casualties in these severely damaged areas, resulting in a lack of people in the area to restore and subsequently maintain the gardens.

Moreover, a comparison of the percentage of roads and passageways existing prior to the earthquake (2003) and after reconstruction (2012) showed an increase of approximately 3 % (Fig. 3.8). In Area 1, which experienced relatively less damage such that buildings remained standing in proper alignment, road widening was achieved by moving back the reconstructed buildings. In Area 3, which experienced major destruction, in addition to moving back the reconstructed buildings, some new roads and streets were built (Fig. 3.9 [c and d]). Roads and open spaces are vital for facilitating transportation and emergency operations in crisis situations. Consequently, the city appears to have become much more resilient as a result of the reconstruction process.

The evaluation of satellite images to determine building changes, discussed in section 4.2, indicated that the ratio of reconstructed buildings increased in proportion to the degree of damage. This correlation suggests that the reconstruction process in the study areas was generally based on the need for change. In other words, we can state that the selection of buildings requiring reconstruction was properly carried out in most cases, with the exception of parts of Area 1, where the ratio of reconstructed units was not correlated with the level of damage. The differences observed within Area 1, which was not severely damaged, could be partially attributed to the bank loan provided by the government (with a 5 % interest rate repayable in 15 years) (Ghafory-Ashtiany and Hosseini 2007). This served to motivate the residents of less damaged buildings to participate in the reconstruction program while benefitting from the aid provided through the loan program.

The relatively large number of vacant lands (111 units out of a total of 623) that were not rebuilt after the earthquake, and subsequent debris removal, suggest that the reconstruction of heavily damaged districts such as Areas 3 and 5 has not yet been completed. Nevertheless, based on the findings of this study, the progress of Bam's reconstruction process, in qualitative and quantitative terms, has been relatively good compared with the post-earthquake reconstruction that took place

in other cities in Iran. For example, during the reconstruction of Manjil after the earthquake that occurred in 1990, little attention was paid to preventing shifts in property boundaries in the city. This had an extensive and negative effect on the official land registry and also led to changes in the social structure (Pooyan 2012). Moreover, during the reconstruction of Manjil, planning that specifically targeted protection of the city's cultural and historical identity was absent. This could have had an important impact on the tourism industry. Even less attention was given to the economic situation, specifically improving living standard and discouraging emigration. Furthermore, despite the construction regulations in earthquake-prone regions, reconstruction continued to be carried out close to fault lines (Mahdi and Mahdi 2013). However, in the case of the Bam earthquake, the previous experience gained from the Manjil earthquake could have led to avoidance of repeating previous mistakes and promoted effective disaster management, including shorter construction times, higher production, and better construction quality.

## 3.6 Conclusions

In this study, we used official statistical data, field survey data, and multi-temporal satellite imagery to evaluate the reconstruction process and land cover changes in the city of Bam after it was struck by a devastating earthquake on December 26, 2003. The study's significance lies in its use of satellite images and remote sensing technologies that have not previously been applied in studies conducted on Bam.

Our results showed that the reconstruction process was adequate in partially damaged districts of the city. However, in severely damaged areas, a sizeable area of vacant land remains despite the implementation of post-earthquake reconstruction. This can be attributed to the destruction of gardens, the deaths of their former owners, and the construction of a number of steel-frame buildings (Fig. 3.3) with smaller footprints.

Our evaluation showed that reconstruction of a significant number of buildings had been completed within 2 to 3 years of the earthquake's occurrence. This indicates that the pace and progress of the reconstruction project was acceptable and that the project was conducted efficiently compared with previous governmental reconstruction projects in Iran. Moreover, a comparison of the building materials and structural types employed in Bam before and after the earthquake

showed that the quality of the building structures had generally improved, probably as a result of direct supervision by the Civil Engineering Organization. It is expected that the new city of Bam will achieve greater sustainability than its predecessor while being much more resilient to future disaster events.

Furthermore, it should be noted that the reconstruction policy formulated for Bam not only responded to the demand for the reconstruction of residential units, but also provided social and urban development and economic growth by establishing new infrastructure, public buildings, and cultural facilities.

In sum, we can conclude that the implementation of Bam's reconstruction plan has been successful, particularly when compared with earlier post-disaster development programs implemented in other cities in Iran. The important factors that contributed to the success of this plan were financial aid and construction materials provided by the government and the active participation of local survivors in the reconstruction process. Although the 2003 Bam earthquake resulted in extensive physical damage and loss of human lives, it led to a rise in national awareness relating to the reduction of risks associated with earthquakes and an improvement in the quality of disaster management in Iran.

Finally, it should be noted that although the analysis of satellite images conducted for this study ensured high accuracy and reduced costs compared with conventional methods entailing field surveys and data collection, the process of manual classification is time consuming and requires considerable expertise. Future work should attempt to develop powerful algorithms to enable automatic and highly accurate detection of types of land cover.

# Chapter 4

# Application of Quad- and Dual-Polarimetric SAR data combination for land-cover detection in desert areas

# 4.1 Introduction

Following the invention of the first digital data sets, significant information has been provided using remote sensing for the classification of land use and land coverage. (Stavrakoudis et al. 2011). A wide range of data with different spatial resolutions to have a rapid urban planning without physical access can be collected by using this technique (Erener, 2013).

Various objects such as water, concrete, asphalt, vegetation, metal and soil are contributed in urban areas, and they have complex nature. Each objective class has different spectral characteristics in RS image (Pacifici et al. 2009). As an example, a simple building which belongs to building class can be interpreted as a complex structure with many architectural details surrounded by trees, gardens, grass, roads, social and technical infrastructure, other buildings, and many other temporary objects.

As it appears in (Amarsaikhan et al. 2007), multispectral remote sensing sources have been widely used for city land-cover detection. But, still there are great challenging tasks due to the complex city texture (Ban et al. 2010). Recently, application of microwave images for urban area classification has become more popular. For classifying, monitoring and analyzing urban aggregates, the SAR images seems essential (Dell'Acqua, 2009, Taubenböck et al. 2012). Thus, development of such a technique for large-area mapping can be considered. The multispectral and microwave images provide different information. Thus, integration those images can efficiently improve urban mapping.

Unlike the passive sensor images, the combined SAR and optical images can observe a particular urban feature. Besides, taking advantage of two sources, they can provide complementary information (Amarsaikhan et al. 2007). Remarkable attempts and valuable progress have been achieved toward the development of new advanced active and passive RS sensors during the last decades. The accurate and detailed mapping of urban land cover and land us should be noted (Hu and Wang, 2013). However, ordinary feature combinations or conventional techniques may not easily separate the complex features in the urban areas, which are diverse in nature and similar in spectral characteristics (K. Roychowdhury 2016).

The atmospheric situation can obstruct the wavelengths of traditional spaceborne optical sensors and multispectral systems, and Radar passes through these circumstances (Stefanski et al. 2014;

Al-Tahir et al. 2014; Henderson et al. 2002). ). Also, since they do not become dependent on the Sun for illumination, they can acquire data at night. These benefits provide radar systems with relevant data selecting potential for many districts, especially those often obscured by persistent cloudy conditions, like tropical and high latitude regions (Sheoran, 2015 and Sawaya et al. 2010).So, the Rada can be a useful and independent source of information for those parts.

Many authors have interpreted their studies that Radar can be fused with optical data to improve land use/cover mapping accuracies(Idol 2015).

For thematic accuracy of classifications, image date is often vital. Thus, it would be quite beneficial for the applications involving green vegetation such as agriculture, forestry, rangeland or wetlands. Scientists often gather detailed information on phenology of natural vegetation and crop calendars, to facilitate the recognition of the best image date for attainment (Niel and McVicar, 2004).

To improve plant discrimination, it has been proven by Le Hegarat-Mascle et al. 2000; Turner & Congalton 1998, that having multiple dates of imagery is very useful. Multidate analysis has been applied by Department of Agriculture, both domestically and in the Foreign Agricultural Office of United States to improve the accuracy of their crop inventories.

 The availability of free imagery, such as from the Landsat and other more recent space-borne missions, facilitate the compilation and acquisition of multi-temporal image datasets. As a result, there are several studies on multi-date analysis for many disciplines. Also, there are many types of research on the application of remote sensing technologies such as hyperspectral imaging (Gomez-Chova et al. 2003; Liu & Bo 2015).As the land use and land cover kinds have variety and complexity, it is often challenging to find unique signatures for each single classes using data extracted for each single band.Compared to radar systems the optical data is quite accessible. Therefore, for most applications, optical data will be the dominant source of imagery

By using multi-date radar or multi-date radar and optical integration, there are several studies confirmed the improvement of crop accuracies (Bargiel & Herrmann, 2011; Yekkihkhay et al. 2014). Multiple image dates improves the accuracies of land use and land cover mapping, and a lot of studies have concentrated on this subject, those researchers demonstrate the importance of

investigating, most of them have focused on comparing differences within the same season and/or the same case study or same classes (Idol et al., 2015).

## 4.2 Study area, Data description, and methodology

## 4.2.1 The study area

In this research, an area of approximately 1600 km2 covering, including all part of Bam city, Baravat city, and Arg-e-Jadid Special Economic Zone. The land covers were studied with a greater focus (more specifically) in the urban areas. This area is located in Kerman province of southeastern Iran, 45 kilometers far from south of Lut Desert (the hottest place on Earth in 2004 and 2005, which reached 70.7 degrees Celsius according to MODIS on NASA's Aqua satellite data (Mildrexler et al. 2006)) and north of Jebal-Barez mountain chain. The area is illustrated in Fig. 4.1.
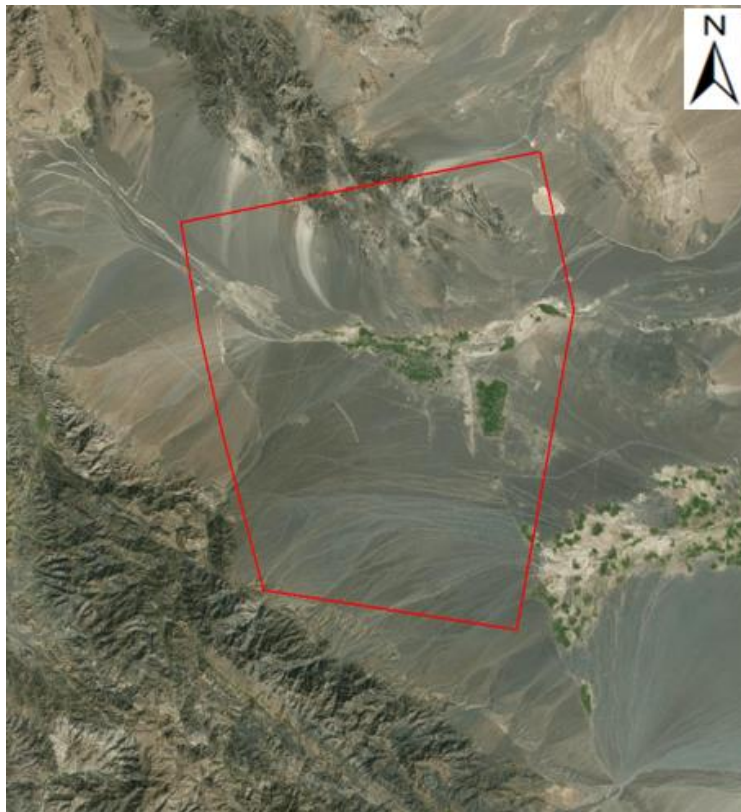


Fig. 4.1 the study area

# 4.2.2 Data Description

Three images were used from two different sensors. Two of these images are from the PALSAR-2 sensor, on ALOS-2 Japanese L-Band satellite launched in 2014. One of these SAR images was an FBD (Fine Beam Dual), 1.1 type, dual polarization (HH and HV), descending product acquired on 27 may 2015. Another one was HBQR 1.1 type, full polarization (HH, HV, VH, and VV), ascending image for seven may 2015. The level-1C image was taken by sentinel-2 satellite used as an optical image in this paper. The image acquired on 30 August 2015 and had 12 multi-spectral bands with 10-m resolution in band red, green, blue and infra-red. The detailed descriptions of these images are given in Table 4.1.

Table 4.1. Detailed descriptions of the images used in the study.

| Sensor Type | Sensor | Product Type | Acquisition Date | Pass | Polarization | Resolution | Antenna Pointing | Off Nadir Angle | Range Spacing | Azimuth spacing |
|---|---|---|---|---|---|---|---|---|---|---|
| SAR | ALOS-2 | HBQR 1.1 | 2015-05-07 | Ascending | Full HH/ HV/VH/VV | 5.54 | Right | 28.4 | 2.861 m | 3.127 m |
| | ALOS-2 | FBDR 1.1 | 2015-05-27 | Descending | Dual HH/HV | 6.6 | Right | 36.6 | 4.291 m | 3.415 m |
| Optical | Sensor | Product Type | Acquisition Date | Pass | Orbit Number | Resolution | Bands | Zenith Angle | Cloud Percentage | Azimuth Angle |
| | Sentinel-2 | S2MSI-1C | 2015-08-30 | Descending | 120 | 10 | 12 | 7.11 | 0 | 103.559 |
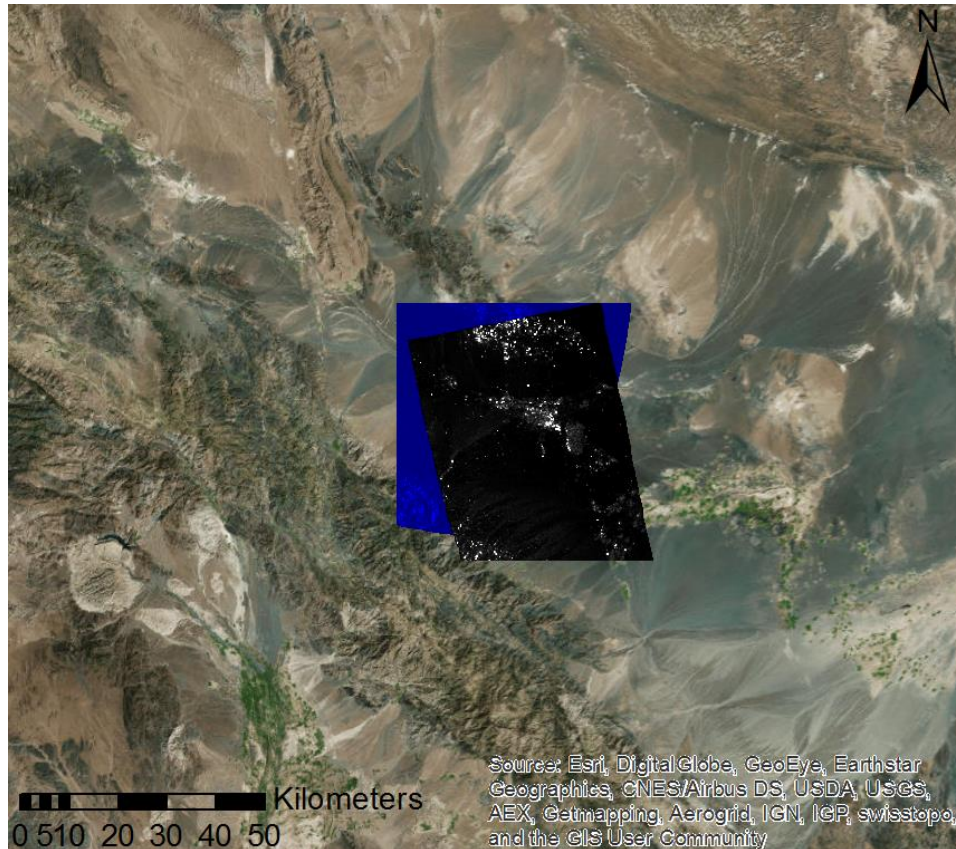
Fig. 4.2 Footprint of SAR data on study area.

## 4.2.3 Methodology

The primary purpose of this research was obtaining the classification of land covers in the arid area by an unsupervised method with the minimum amount of operator interfere. To achieve this goal, we used a combination of two SAR image which was taken by ALOS-2 and one optical image which was taken by Sentinel-2 satellite. A flowchart of the methodology is shown in Fig. 4.3.
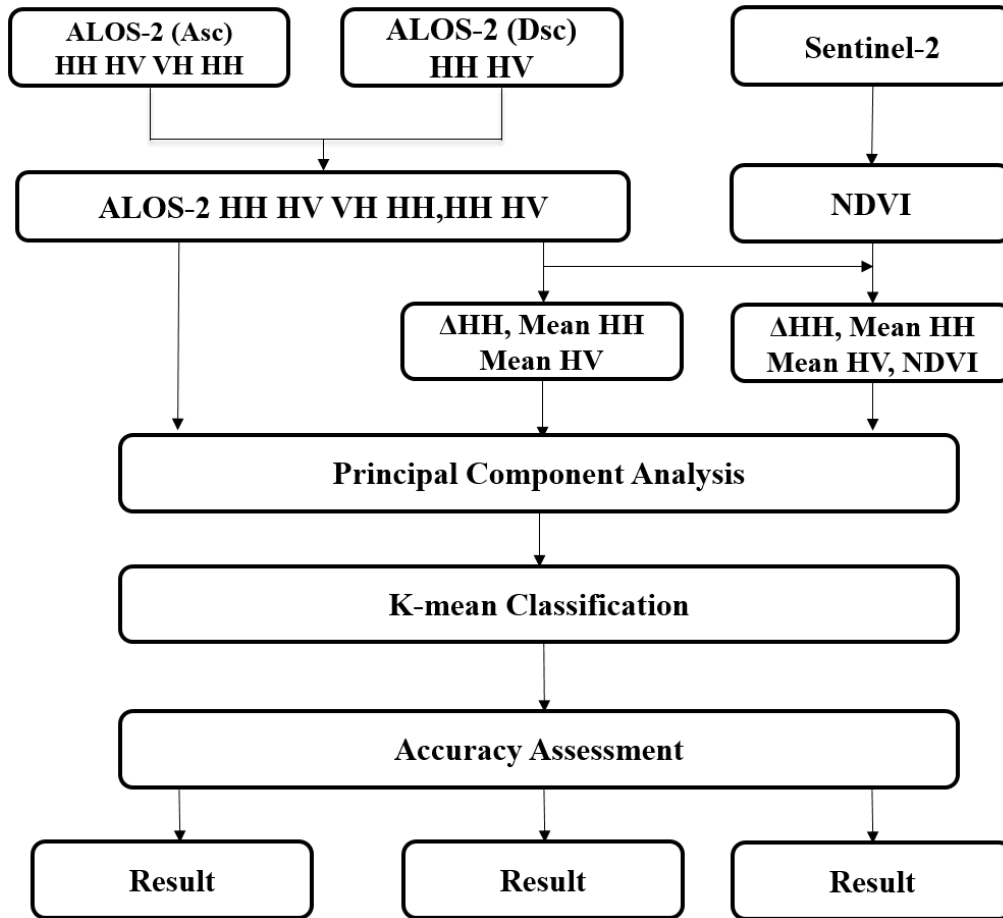
ALOS-2 (Asc)
HH HV VH HH

ALOS-2 (Dsc)
HH HV

Sentinel-2

ALOS-2 HH HV VH HH,HH HV

NDVI

ΔHH, Mean HH
Mean HV

ΔHH, Mean HH
Mean HV, NDVI

Principal Component Analysis

K-mean Classification

Accuracy Assessment

Result

Result

Result

Fig. 4.3 flowchart of the methodology.

We chose one of the SAR images with ascending path and another in descending path to improve a detection of objects (especially buildings) which located in different directions. Fig. 4.9 shows objects with high backscatter values in ascending path in red and objects with high backscatter values in descending Path in cyan.

Two SAR images were stacked together after preprocessing level which was explained precisely in section 4.3. The final product in this step is a combination of 6 bands (HH, HV, VH, VV, HH, and HV) with 6.6-meter resolution. In figure 4.8, the color composite of this sample product is introduced, where they are R; Band HH 7 may, G; Band VV 7 may, B; Band HH 27 may.

To have the best classification in this research, three evolutionally processes (to improve the previous method) and based on 6-band images DATA are performed.

# 4.3 SAR data pre-processing

The SAR images were provided as the FBD and HBQR data with the processing level 1.1 ALOS-2, which are represented by the complex I and Q channels to preserve the amplitude and phase information( Fig 4.4 and 4.5). After several pre-processing steps using the SNAP Desktop software, these images were projected on the WGS84 reference ellipsoid with a pixel spacing of 6.6 m. For speckle reduction, microwave data needs to be filtered. Lee Sigma filter with 5*5 pixel window size and 0.9 sigma factor was applied to reduce speckle noise (Kato and Yamazaki, 2008).



Intensity HH     Intensity HV     Intensity VH     Intensity VV
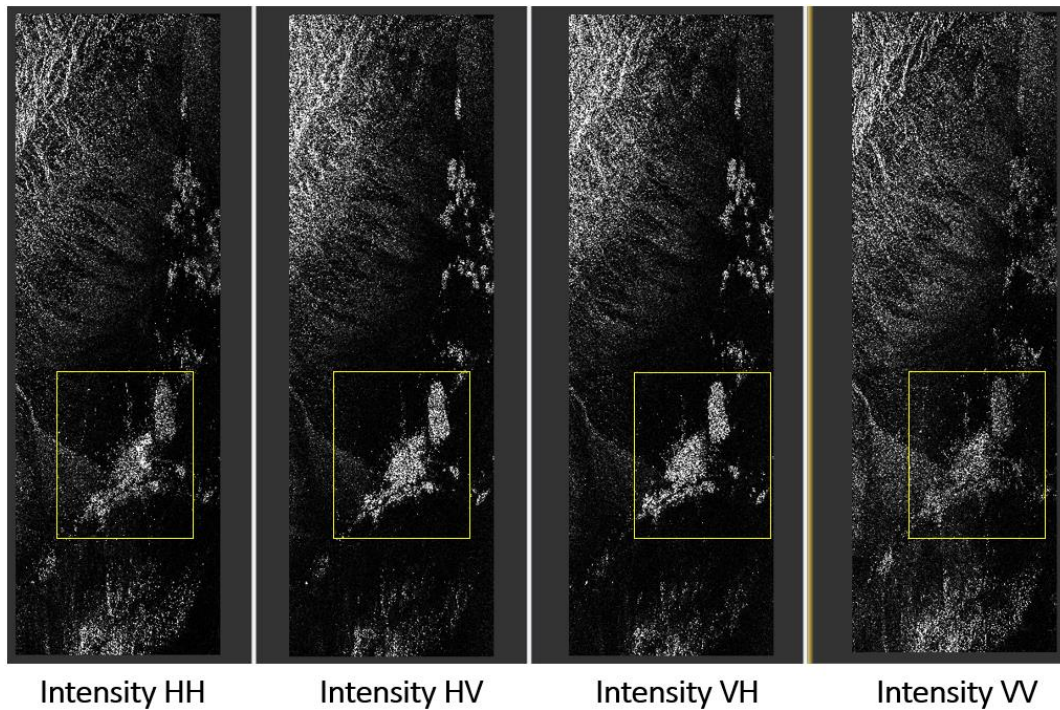
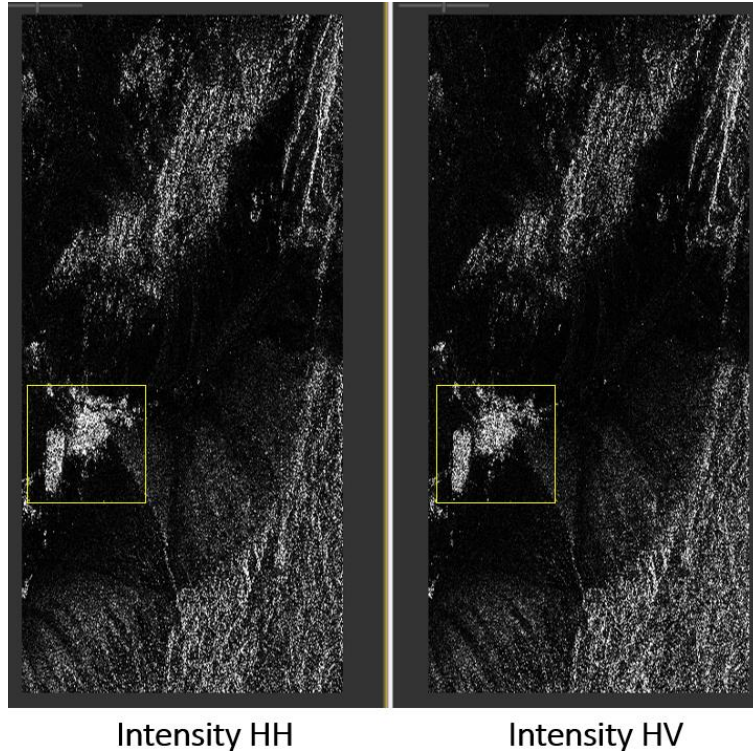Fig. 4.4 ALOS-2 HBQR data with the processing level 1.1 captured on May 7 and the location of Bam city.

Fig.4.5 ALOS-2 FDB data with the processing level 1.1 captured on May 27 and the location of Bam city.

Radar images are made up of digital numbers characterizing the intensity of the back-scattered energy for each pixel. The contrasted the back-scatter from different objects enables them to be visually discriminated. The datasets of both images were radiometric calibration to achieve sigma nought ($\sigma°$) or the backscatter values in the ground range with the decibel (dB) unit, represented by the following equation:

$$\sigma° \text{ (dB)} = 10\log(DN/10) \tag{4.1}$$

Where DN is the digital number of backscattering intensity of SAR images. After this conversion, bilinear interpolation resampling type of calibration was applied to the images. Then both the images were terrain corrected and stacked.
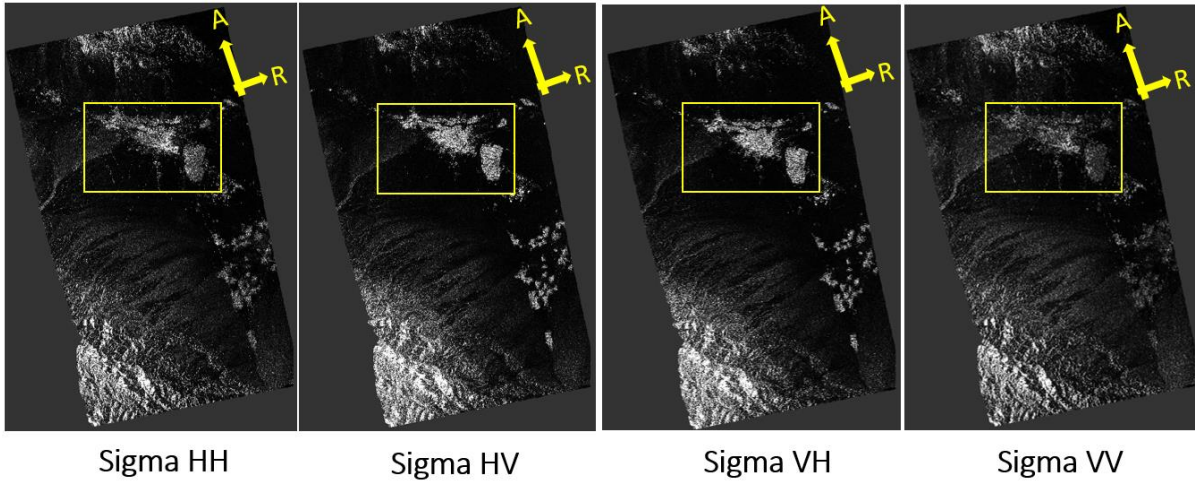
Sigma HH    Sigma HV    Sigma VH    Sigma VV

Fig. 4.6 ALOS-2 HBQR data captured on May 7 after preprocessing and the location of Bam city.
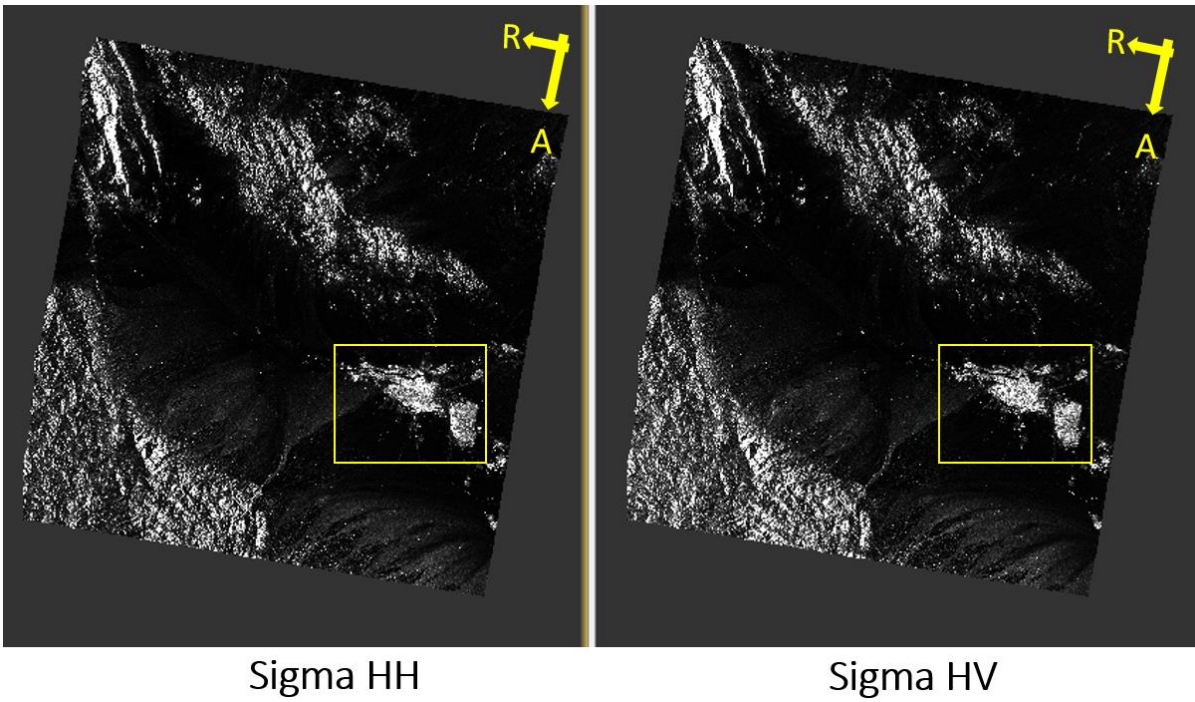


Sigma HH                    Sigma HV

Fig. 4.7. ALOS-2 FBD data captured on May 27 after preprocessing and the location of Bam
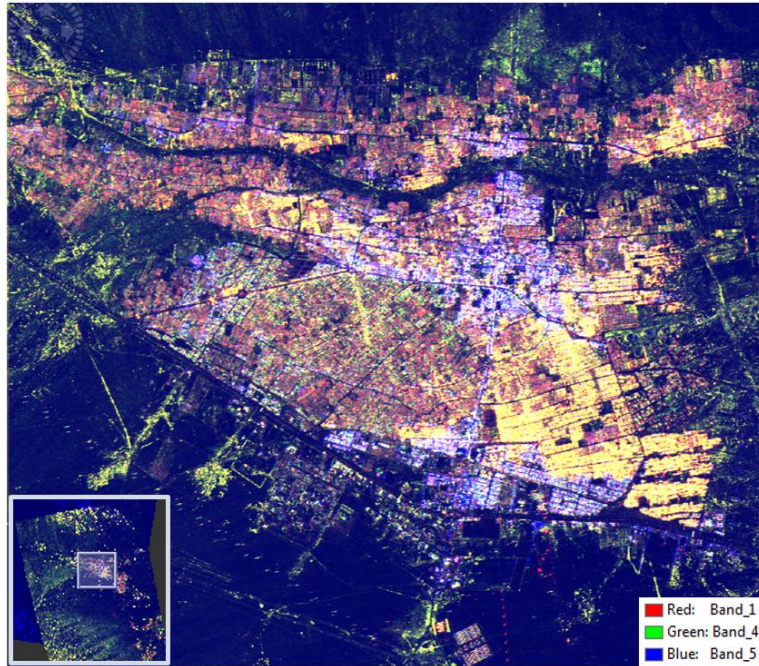
Fig 4.8. Band composition, Red: Sigma HH 07 May 2015(Ascending) Green: Sigma VV 07 May 2015 (Ascending) Blue: Sigma HH 27 May 2015(Descending)
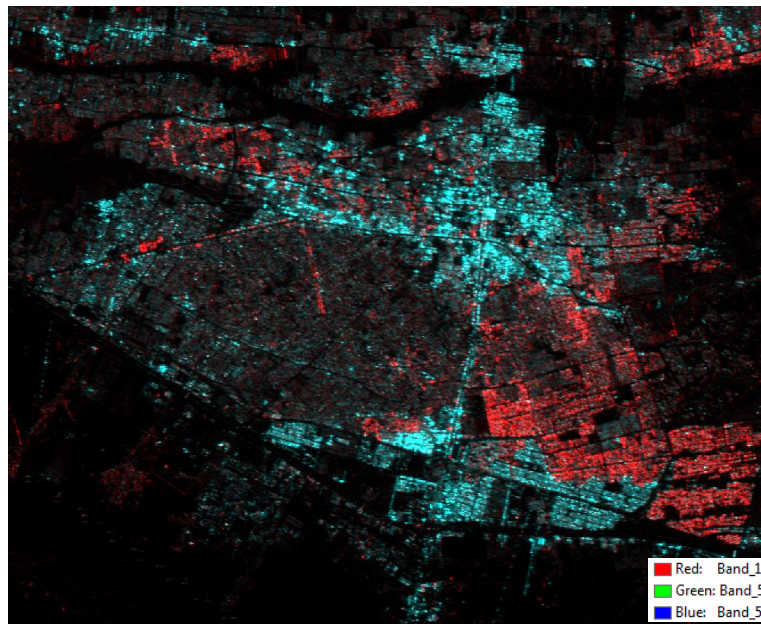


Fig 4.9. Band composition, Red: Sigma HH 07 May 2015 (Ascending), Green and Blue: Sigma HH 27 May 2015 (Descending)

## 4.4 Backscatter value diagrams

We provided the land covers signature value diagrams to realize the statement of backscatter value of each pixel in a particular image according to the related land cover of that pixel. For this purpose, 231 samples from all Land Covers type with the whole area xm2 from the Sentinel-2 image with ten-meter resolution were selected (as shown in fig. 4.10). We tried all kinds of colors, heights, and angles of objects to be included in the sample selection. Subsequently, we achieved backscatter value ranges for each land cover in different images by determining the related backscatter value.
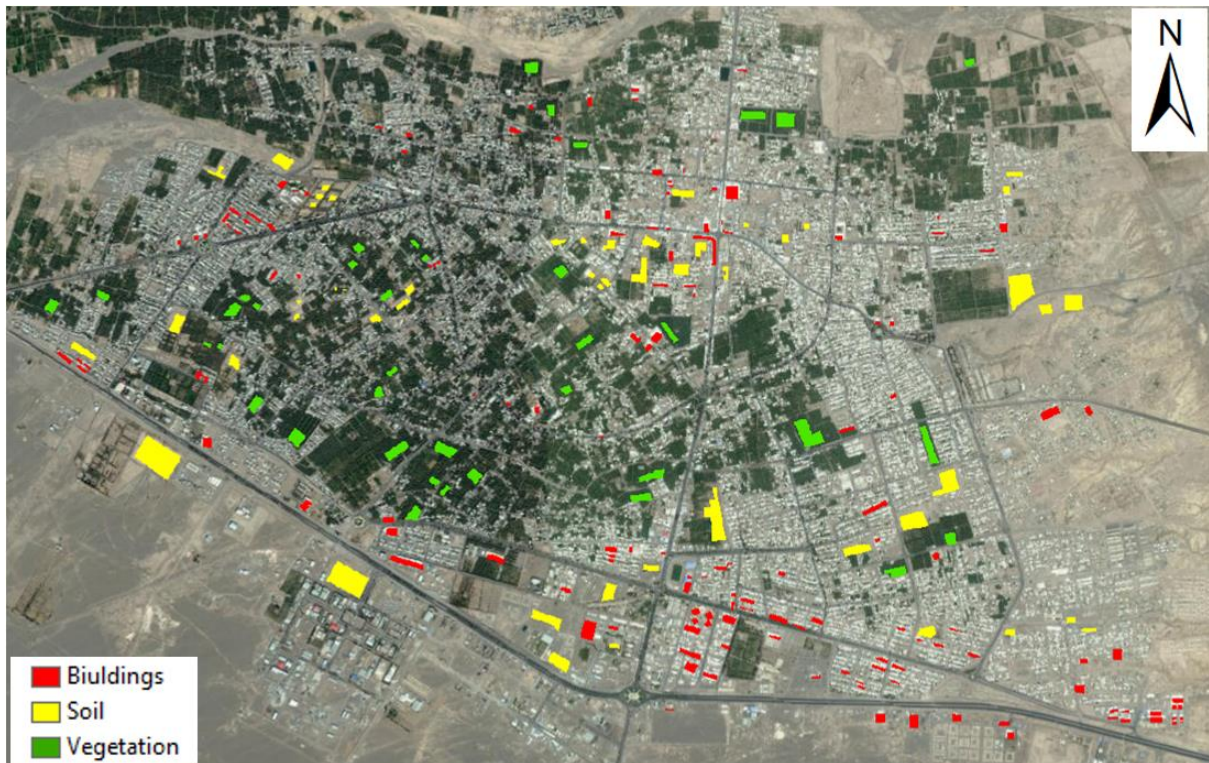


Fig. 4.10 samples of all land cover types for backscatter value diagrams.

## 4.5 Research process

## 4.5.1 Multi-polarization SAR data

In the first method, The six bands of two images were layer stacked, PCA for 6 Band images is performed and then on three first component classification was done. To identifying the classes,

Backscatter values (σ°) were used. The K-Means method was performed for the classification scheme. (Chipman et al., 2004).

To have the best result in classification, we started with 40 different classes, and we changed threshold to 99% of the total. The resultant classes merged to the following three major land cover classes: Buildings, bare land, and vegetation. Then, training sample datasets were created to be applied for the classification of images. (Fig. 4.15).
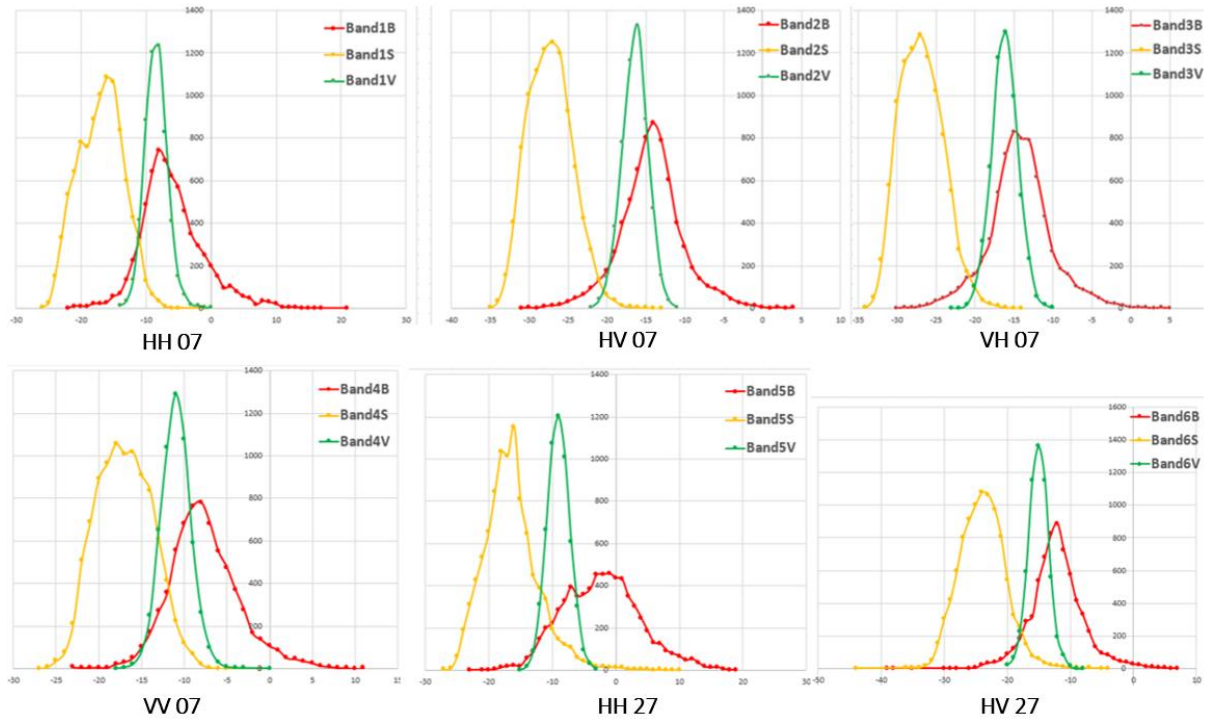


Fig. 4.11 The land covers backscatter values histogram for the six bands of SAR images.
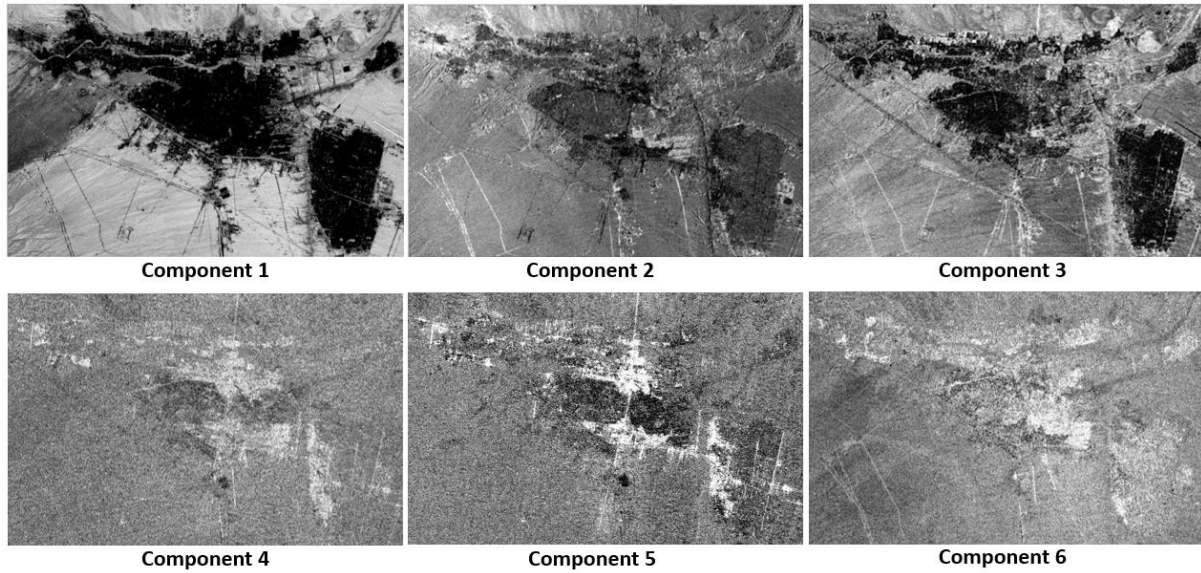
Fig. 4.12. Principal component analysis results (6 bands from two SAR images)

Figure 4.11 shows the signature value diagram for each one of 6 bands taken by ALOS- 2. The red lines refer to Buildings, yellow lines to Soil and Green to Vegetation. It is evident, in all images except HH may 27, there are many similarities in backscatter values diagram of Building and Vegetation land covers, while the diagrams relating to the backscatter value of Soil is appropriately different. These diagrams explain why the initial classification misclassified most of the Building as the Vegetation and vise verse. As is shown in figure 4.13, performing PCA (Fig 4.12) almost decreased the difficulty, and the deviation between Vegetation and Buildings diagrams is enlarged in the first component.
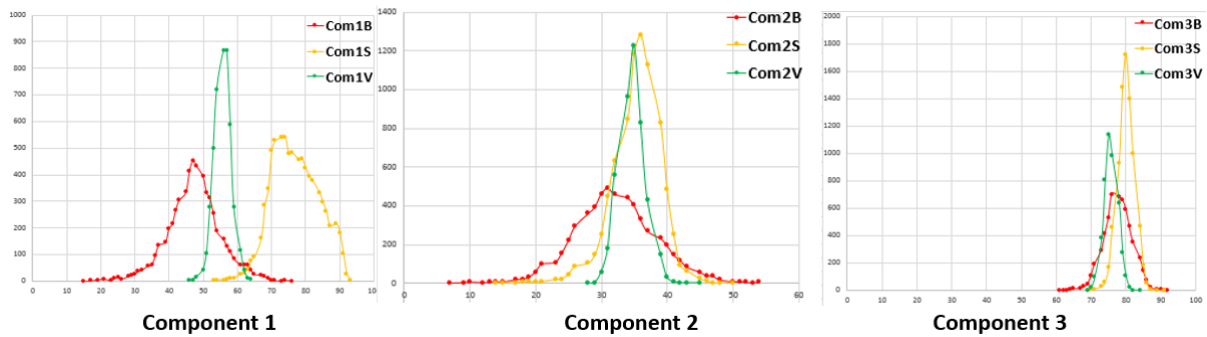


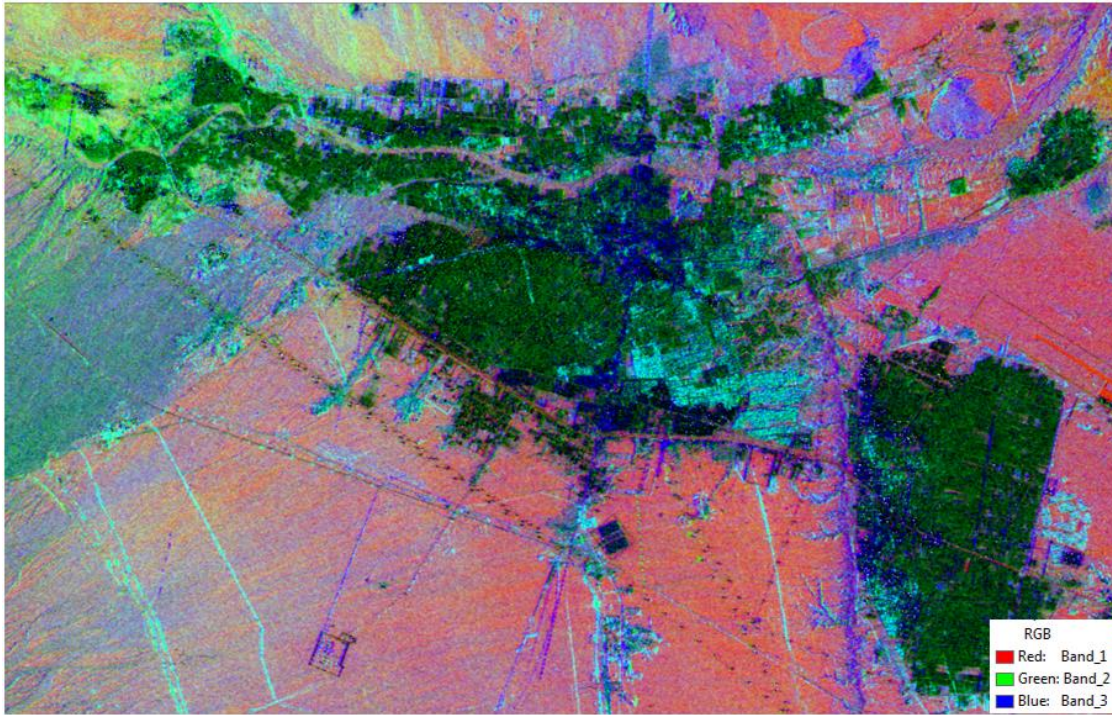Fig. 4.13 The land covers backscatter values histogram for the first three components.

Fig. 4.14 Bands color composition for principal component analysis results, Red: Component 1, Green: Component 2, Blue: Component 3
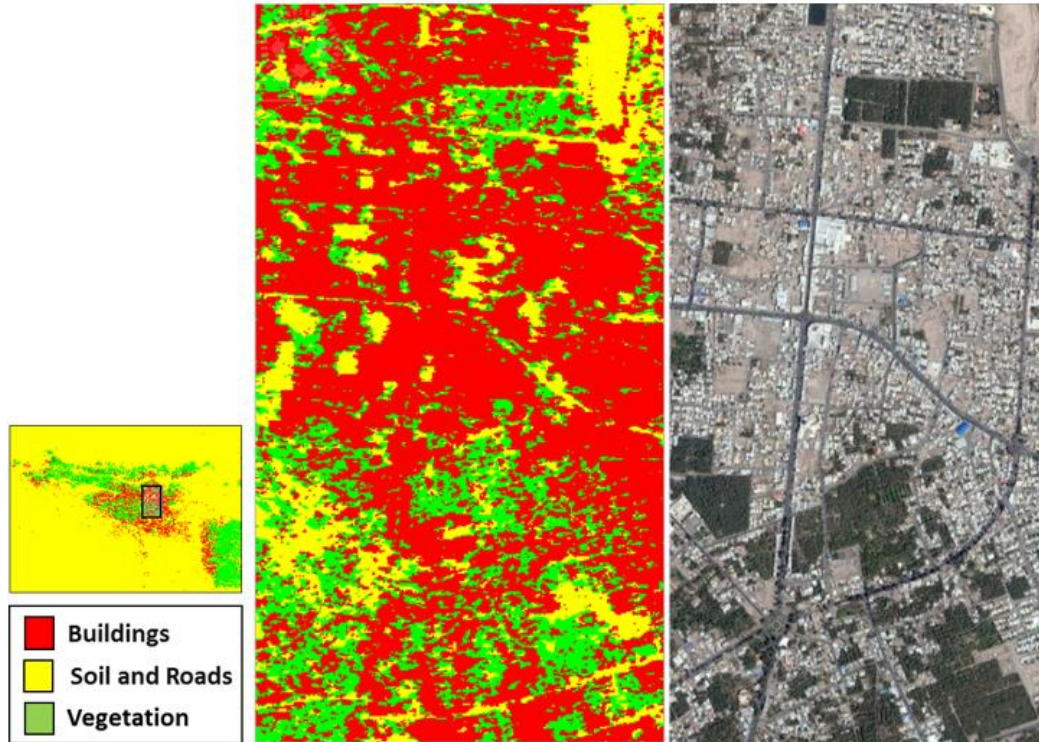


Buildings
Soil and Roads
Vegetation

Fig. 4.15 K-means unsupervised classification for three components of six bands, 40 Classes, Merge to 3 classes.

## 4.5.2 ΔHH, Mean HV, Mean HH

In this part, we reduced the number of active bands to noise reduction and then having a better classification. For this purpose, first the mean of sigma naught value for the both equivalent pixels in HH band may 27 and May 07, and mean of sigma naught Value for the both equivalent pixels in HV may 07 and May 27 are evaluated. Also, the difference between sigma naught value for the both equivalent pixels in HH band May 07, and HH May 27 are estimated (Liu et al., 2012; Liu et al., 2014).

$$\Delta HH = HH_{Asce} - HH_{Desc}$$
$$Mean\ HH = (HH_{Asce} - HH_{Desc})/2$$
$$Mean\ HV = (HV_{Asce} - HV_{Desc})/2 \qquad : 4.2$$
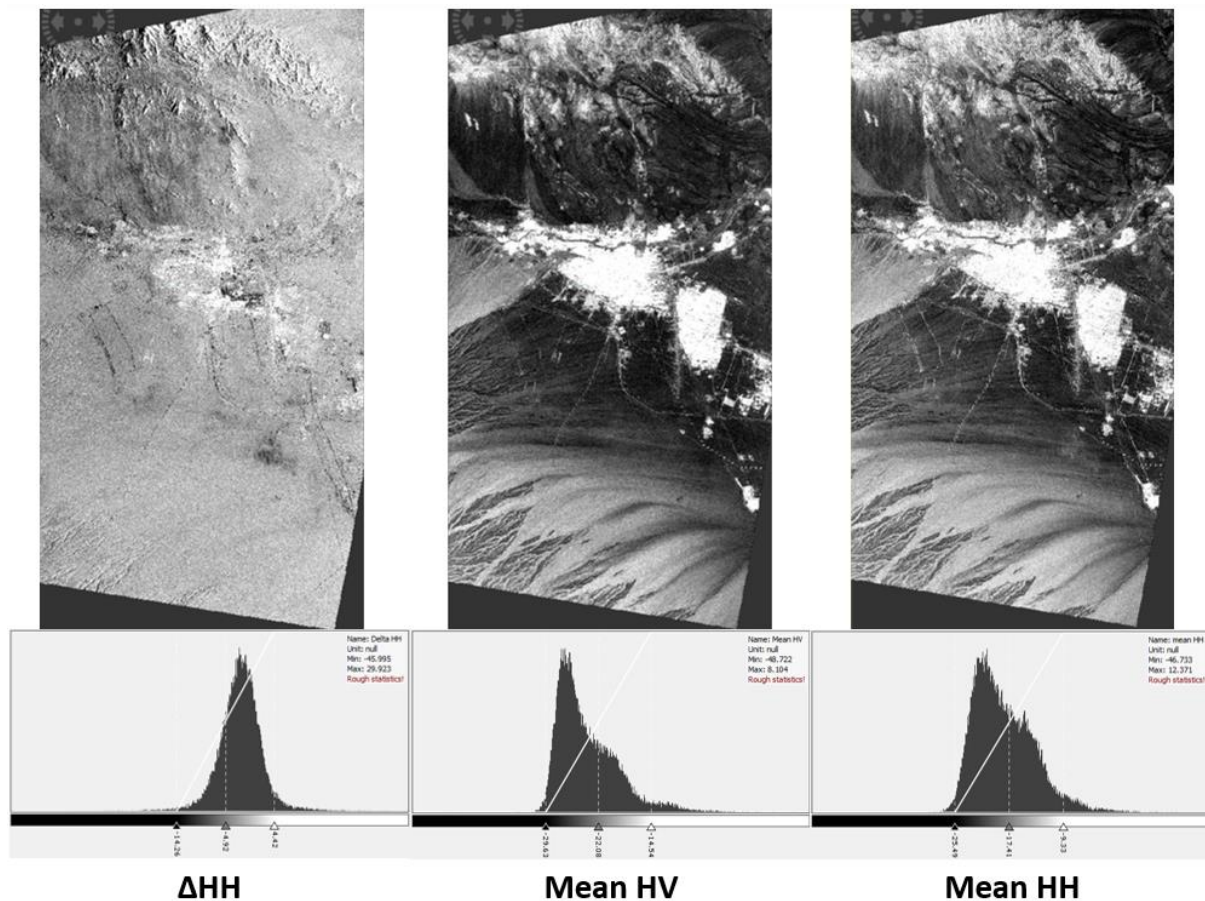


Fig. 4.16 Backscatter value analysis (ΔHH, Mean HV, Mean HH) results and histograms.

Three new nominated images (ΔHH, mean HV, mean HH) are stacked together (Fig. 4.17). Then PCA for this new 3-Band image was performed (Fig. 4.19), and the first two components K-mean classification was conducted (Fig. 4.19).



Component 1          Component 2          Component 3
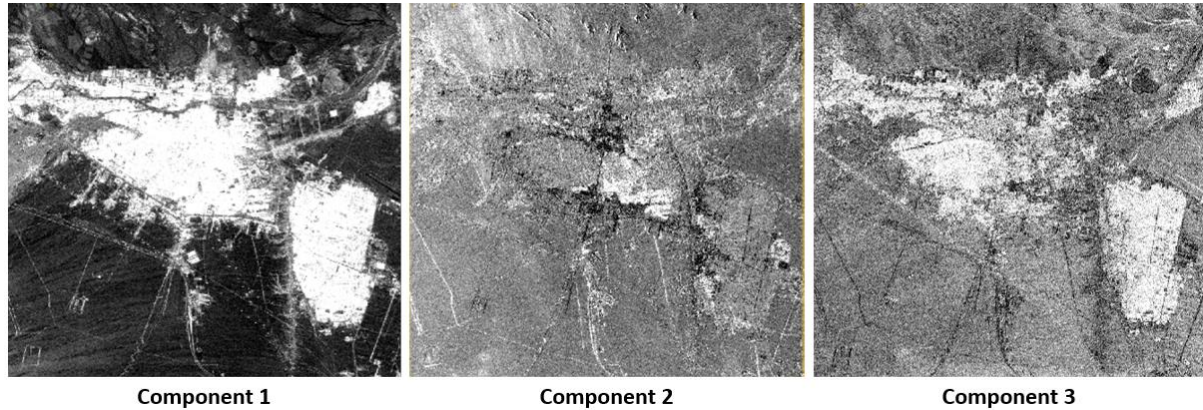
Fig. 4.17 Principal Component Analysis for ΔHH, Mean HV, Mean HH
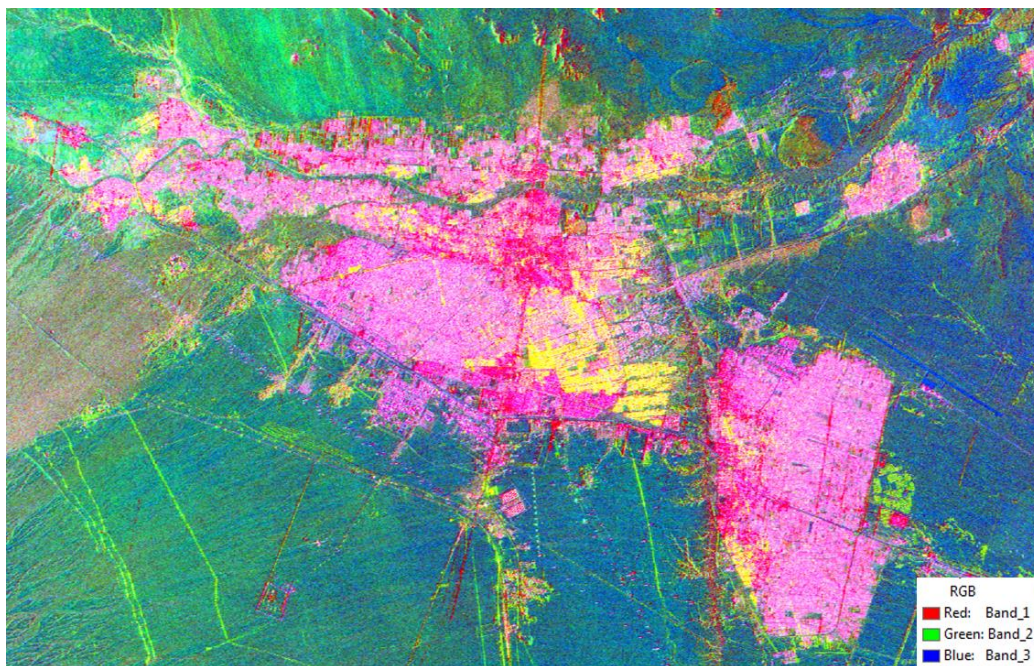


Fig. 4.18 Bands color composition, PCA for ΔHH, Mean HV, Mean HH, Red: Component 1, Green: Component 2, Blue: Component 3
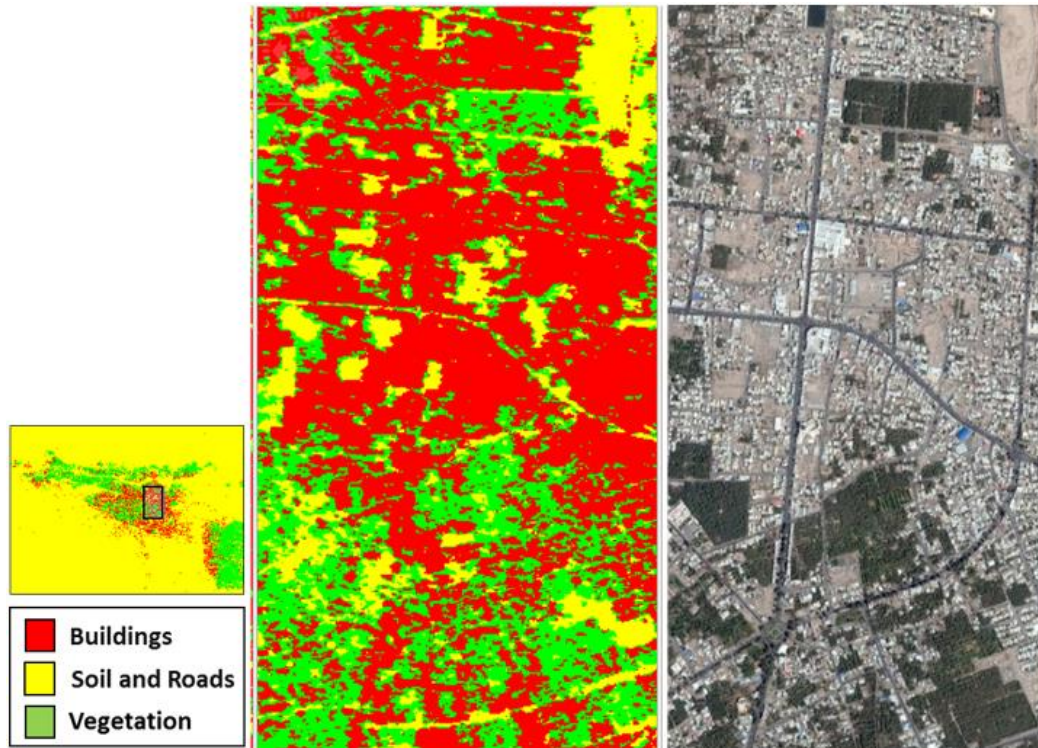
Fig. 4.19 K-means unsupervised classification for two components of ΔHH, Mean HV, Mean HH bands, 40 Classes, Merge to 3 classes.

# 4.5.3 ΔHH, Mean HV, Mean HH, NDVI

For increasing the accuracy of the results in the third method SAR, and optical images were combined. Vegetation land covers can be detected by optical images well, especially via Red and Infrared bands.

## 4.5.3.1 Optical data processing

The optical data was download from the ESA (European Space Agency) website, and it was used to produce NDVI image of the region. By spectral indices which could be employed as features the Sentinel 2 image was described, then as we explained before these indices use the values from two bands to calculate an index that represents the pixel.
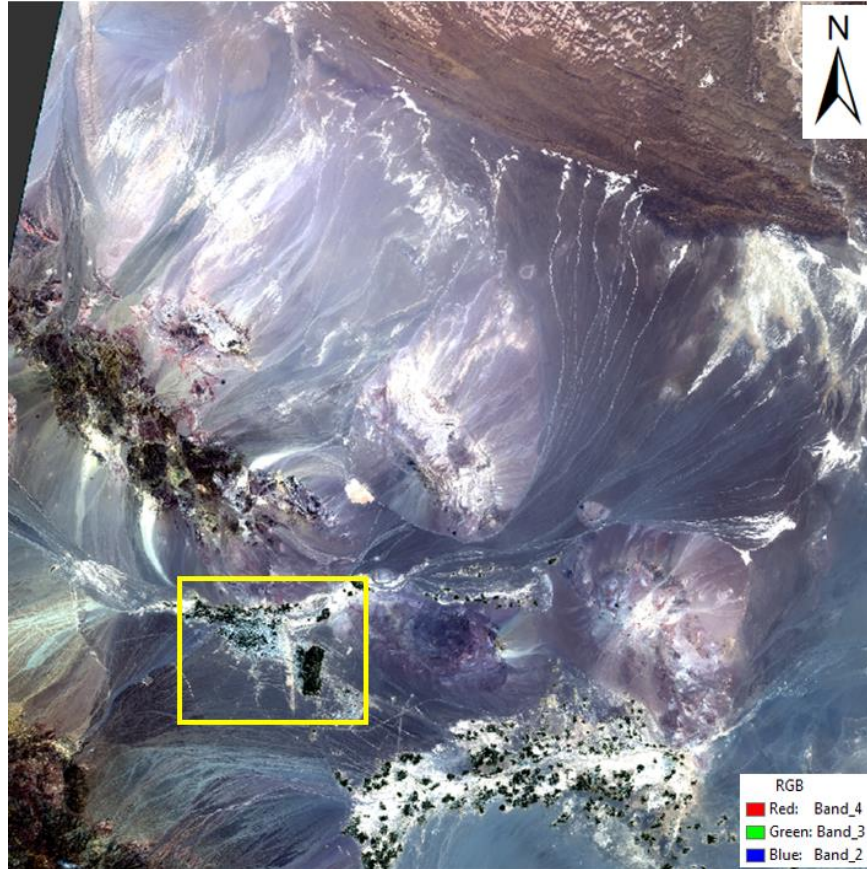
Fig. 4.20. Sentinel-2 image, captured on 2015 august 30

The indices are designed to accentuate some particular land cover class. The Normalized Difference Vegetation Index (NDVI) characterizes live green plant. It was first introduced by Rouse et al. (1973). The index uses the visible red band and the near-infrared band, and is calculated as follows:

$$NDVI = \frac{(NIR - Red)}{(NIR + Red)}$$

**: 4.3**

Where RED corresponds to surface reflectance in Sentinel-2 band 4 and NIR corresponds to surface reflectance in Sentinel 2 band 8. This index works with the principle where vegetation results in a large difference in the two used bands. This leads to large NDVI values (Monica Sandberg 2015).

# 4.5.3.2 Fusion of optical and SAR images

The image fusion technique aims at integrating the information conveyed by data acquired with different sensors, also spatial and spectral resolutions, for purposes of image analysis, feature extraction, modeling, and land cover classification (POHL and VAN GENDEREN, 1998). To allow for joint processing and interpretation of ALOS-2 and Sentinel-2 data the following pre-processing steps were performed· First, the bands of the S-2 product were brought to the same resolution (6.6 m). This procedure accounted for the fact that our Alos-2 products have 6.6m x 6.6m pixel spacing after preprocessing. After that, the SAR image bands were stacked with Sentinel-2 data (NDVI) using nearest neighbor approach. Next, the area of interest was selected, and both datasets were cropped to the same area of interest surrounding Bam city. Finally, to ensure that the same ground sampling grid is employed in both datasets the SAR data was resampled to reach the same number of pixels as the optical data.

Accordingly, first by using NDVI method, land Covers relating to the vegetation discovered, then we combined this result as a band with the other three bands (ΔHH, mean HV, mean HH, mean HV). After principal component analysis performance for above combination, the most three influenced components (Fig. 4.21) were selected, and K-mean method was used for an unsupervised classification (Fig. 4.23). Finally, by comparing the result of the classification and the truth data, confusion matrices were built to accuracy estimation for the method (Table 4.5).



**Component 1**        **Component 2**        **Component 3**
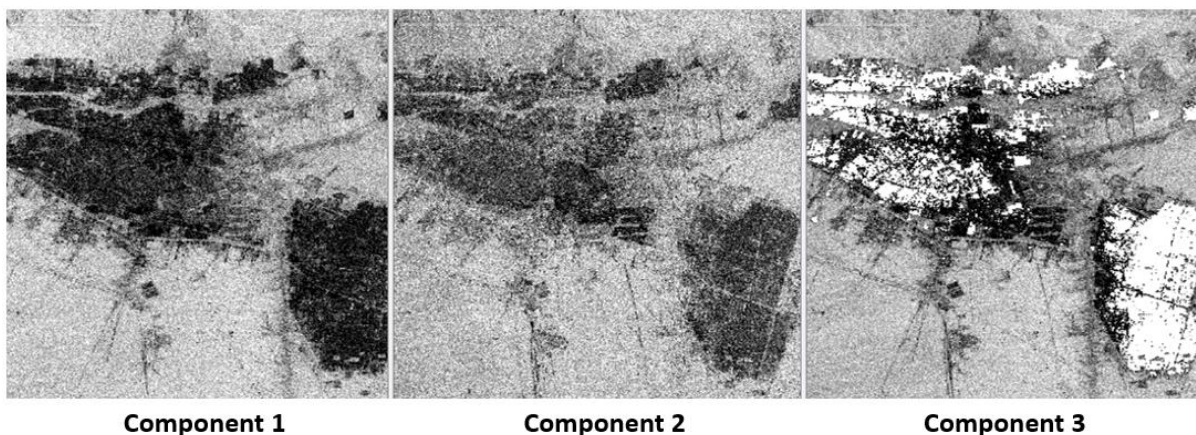
Fig. 4.21 Principal Component Analysis for 4 bands (ΔHH, Mean HV, Mean HH, NDVI).
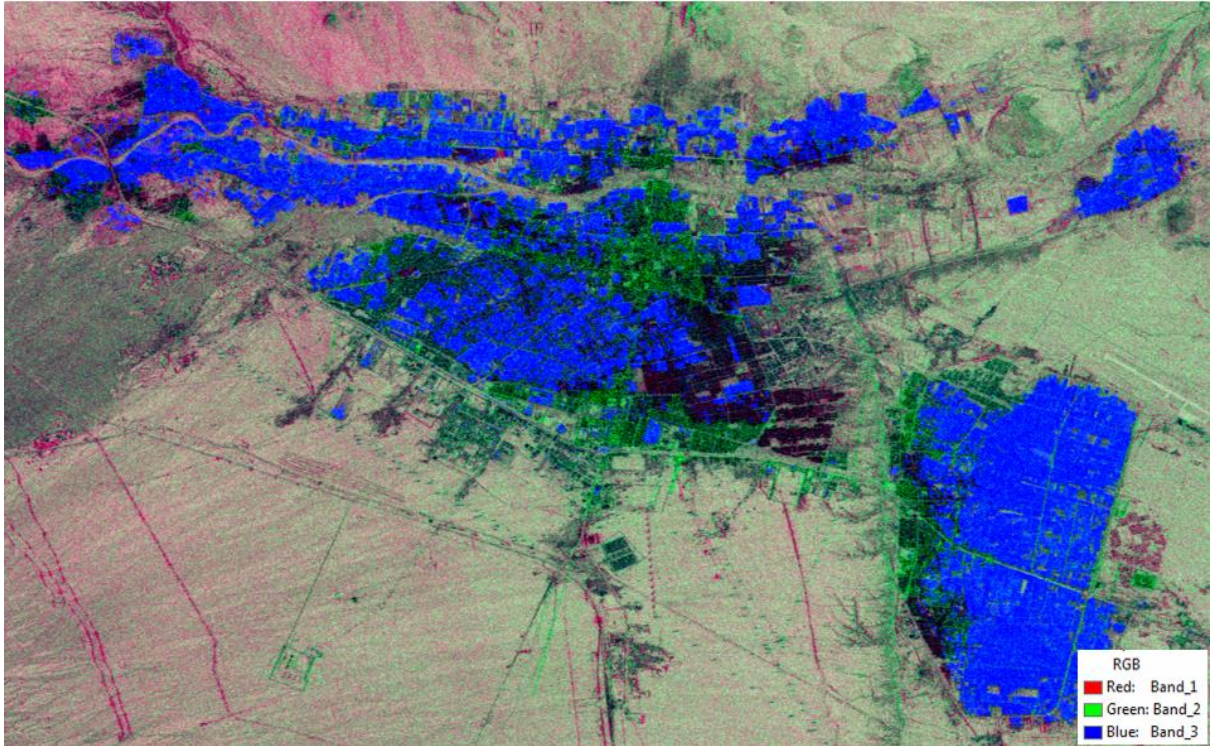
Fig 4.22 Bands color composition, PCA for ΔHH, Mean HV, Mean HH, NDVI, Red: Component 1, Green: Component 2, Blue: Component 3.

To make a larger difference among the diagrams and having a most accurate classification, the final land covers signature value chart as shown in figure x, have built after performing the process as explained. According to the designed process, diagrams of different land covers (especially in the third component) is thoroughly characterized, and intersections and confusions between Vegetation and Building are nicely improved, and an excellent classification can be expected.
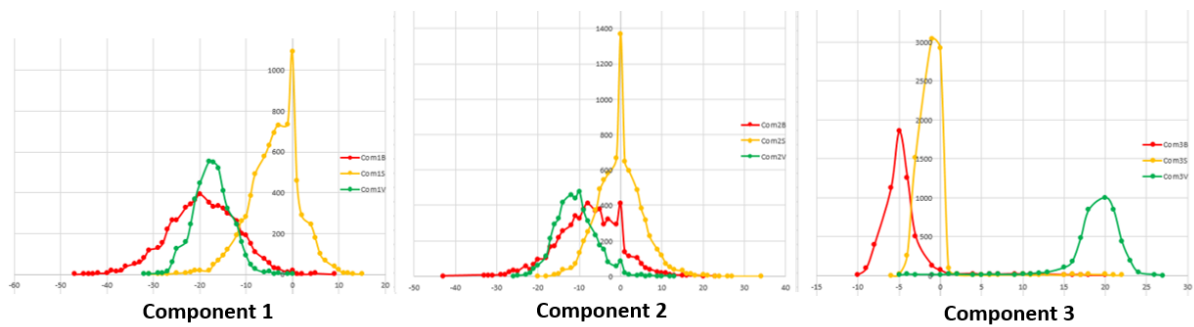


Fig. 4.23 The land covers backscatter values histogram (ΔHH, Mean HV, Mean HH, NDVI) for the first three components.
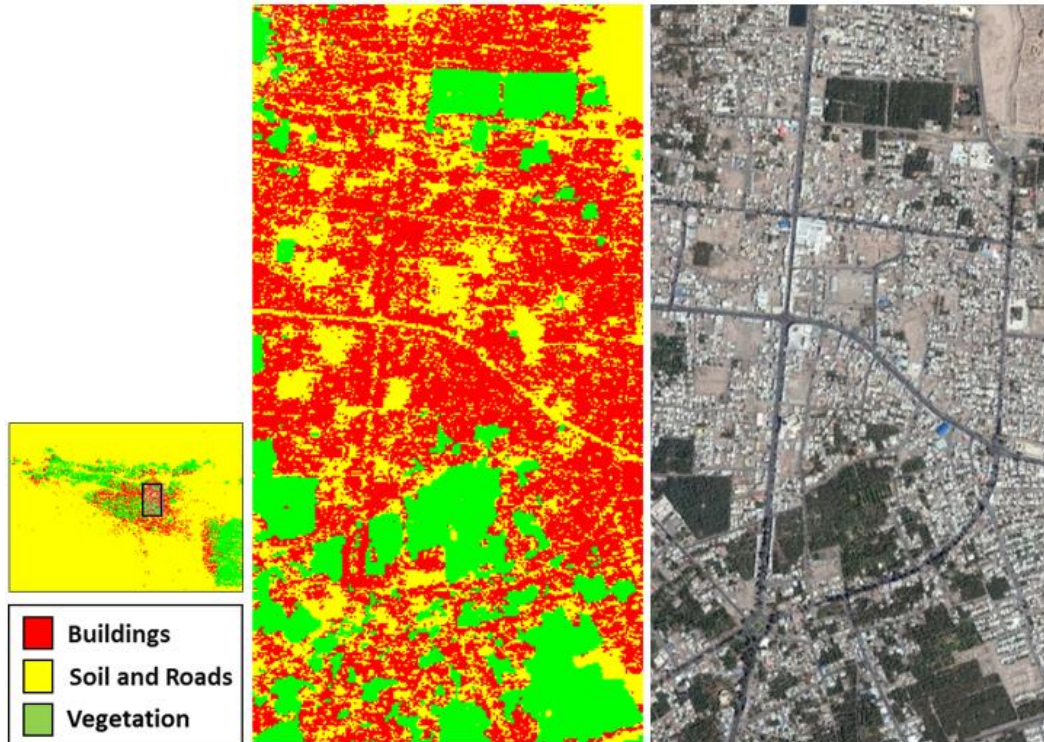
Fig. 4.24 K-means unsupervised classification for three components of ΔHH, Mean HV, Mean HH and NDVI bands, 40 Classes, Merge to 3 classes.

# 4.6 Result Evaluation

## 4.6.1 Training Phase

The training and test data sets for this study were created manually with the primary reference image, the high-resolution GeoEye-1 image. For each class, three samples of truth data with 150m x 150m size were used (Fig. 4.25). These samples were selected according to the resolution of the optical image (10 meters) and local urban block scale. The samples have been chosen randomly from different parts of the city as much as possible.

Fig 4.25. The samples of truth data, size: 150m x 150m

# 4.6.2 Accuracy Assessment\Confusion Matrix

Confusion matrices have been applied to validate the classification results and calculate various accuracies. This matrix has been computed for each classification map, and it also has been included values for the final accuracy of the producer and the user, in this study, the confusion matrix used the test plots that were manually defined at an earlier stage. The test plots could lead to different results. By the same amount of test pixels per class give an overview of the results for each class Hence for final validation of the results it should be taken into account (Sandberg 2015).

Table 4.2 Confusion matrix, PCA of 11 bands optical image

| | | Truth data | | | | |
|---|---|---|---|---|---|---|
| | | Buildings | Soil | Vegetation | Classification overall | Producer Accuracy (%) |
| Classifier results | Buildings | 901 | 654 | 0 | 1555 | 57.94 |
| | Soil | 635 | 933 | 2 | 1570 | 59.42 |
| | Vegetation | 0 | 0 | 1516 | 1516 | 100 |
| | Truth overall | 1536 | 1587 | 1518 | 4641 | |
| | User Accuracy (%) | 58.65 | 58.79 | 99.86 | | |
| | Overall accuracy (OA): | 72.183% | | | | |
| | Kappa | 0.583 | | | | |

Table 4.3 Confusion matrix, PCA of 6 Polarization SAR Image

| | | Truth data | | | | |
|---|---|---|---|---|---|---|
| | | Buildings | Soil | Vegetation | Classification overall | Producer Accuracy (%) |
| Classifier results | Buildings | 1157 | 165 | 202 | 1524 | 75.91 |
| | Soil | 18 | 1349 | 206 | 1573 | 85.76 |
| | Vegetation | 366 | 73 | 1110 | 1549 | 71.65 |
| | Truth overall | 1541 | 1587 | 1518 | 4646 | |
| | User Accuracy (%) | 75.08 | 85.01 | 73.12 | | |
| | Overall accuracy (OA): | 77.83% | | | | |
| | Kappa | 0.667 | | | | |

Table 4.4 Confusion matrix, PCA of ΔHH, Mean HV, Mean HH

| | | Truth data | | | | |
|---|---|---|---|---|---|---|
| | | **Buildings** | **Soil** | **Vegetation** | **Classification overall** | **Producer Accuracy (%)** |
| **Classifier results** | **Buildings** | 1296 | 45 | 198 | 1539 | 84.21 |
| | **Soil** | 4 | 1452 | 78 | 1534 | 94.65 |
| | **Vegetation** | 241 | 90 | 1242 | 1573 | 78.95 |
| | **Truth overall** | 1541 | 1587 | 1518 | 4646 | |
| | **User Accuracy (%)** | 84.10 | 91.49 | 81.81 | | |
| | **Overall accuracy (OA):** | 85.88% | | | | |
| | **Kappa** | 0.788 | | | | |

Table 4.5 Confusion matrix, PCA of ΔHH, Mean HV, Mean HH, NDVI

| | Truth data | | | | |
|---|---|---|---|---|---|
| | **Buildings** | **Soil** | **Vegetation** | **Classification overall** | **Producer Accuracy (%)** |
| **Buildings** | 1327 | 69 | 0 | 1396 | 95.05 |
| **Soil** | 214 | 1518 | 0 | 1732 | 87.64 |
| **Vegetation** | 0 | 0 | 1518 | 1518 | 100 |
| **Truth overall** | 1541 | 1587 | 1518 | 4646 | |
| **User Accuracy (%)** | 86.11 | 95.95 | 100 | | |
| **Overall accuracy (OA):** | 93.90% | | | | |
| **Kappa** | 0.909 | | | | |

# 4.7 Results and Discussion

The land cover classification of optical images based on some algorithms which are configured on Pixels Features. Many software will detect different classes wrongly the same one when having almost similar pixel color. (Although by using object-based classification this error can be decreased, it is not considered here). The Sentinel-2 Satellite Image has been considered as an optical sample for Land Cover Classification and k-mean unsupervised method with 40 minimum class size, and 20 sample interval factor has applied as a classification method in this research. The number of outputs is defined 40 and after the classification Merged to 3 categories; Vegetation, Soil, and Building.

For the accuracy check, three districts from each class (with a size 22500 m2 for each one) were selected randomly, and producing maximum error matrix. As can be seen in Figure x the accuracy of optical image classification for the Soil and Building were small and approximately 60 percent. However, the overall accuracy has increased to 72.18 percent because of high accuracy of discrimination of vegetation in the optical images.

In this product, more than half of pixels relates to the soil have been wrongly realized buildings, and more than half of pixels belonging to the building have been incorrectly achieved as soil. The variety of soil type and matching their color with the color of construction materials in the buildings in this kind of desert district is the primary reason for these significant errors. To solve this difficulty we have used SAR images.

Comparing the exactness of the results were applied in different methods in this research, indicates that the combination of 4-bands, NDVI, ΔHH, mean HV, mean HH have the highest accuracy. Table x shows the accuracy of the 6-banded combination methods; HH, HV,  VV and VH polarization from the image taken on May 7 and HV,  HH  polarization from the image taken on May 27.

In this method, the smallest accuracy is for the Vegetation, 23.63 percent of Vegetation have realized Building, and 4.71 percent of Vegetation have realized Soil. Also, 13.25 percent of Buildings have been realized Vegetation. As has been indicated in figure x, the main reason for this deviation is the intersection and closeness of Backscatter values of these land covers in the SAR images.

We obtained the average value of each equivalent pair pixels in two HH and two HV bands and also the difference value of each equivalent pair pixels in two HH bands, to improve the accuracy of the classification results and increase the separatability of the each land cover diagram as we comprehensively illustrated in previous sections.

This process increased 8 percent in overall accuracy; 5 percent in Building, 9 percent in Soil, and 7 percent in Vegetation. Although similar to the previous method the Backscatter Value for Land Cover, Building and Vegetation were too close or had an intersection, such that about 15 percent of Vegetation were wrongly realized Building and 12.86 percent of Building were incorrectly recognized Vegetation.

# 4.8 Conclusion

This study intends to perform a combination of optical and active microwave images to improve the land cover classification for arid areas conditions. Also, to increase the effect of the vegetation on the SAR images and to better classify the radar data, the optical data are also incorporated.

Dryland environments such as arid and semi-arid environment contain a significant amount of the global population and are sensitive to environmental changes. Considering the land change in dryland areas, the land cover mapping can be served to observe and analysis the administrative decisions on land utilization for different goals. Land cover plans are a fundamental topic in urban sciences. Also, they are the significant data source for investigating the city and environmental changes.

In this decade, land cover change`s monitoring depends on remote sensing images and technology. Different techniques can be performed for classifying land use from satellite products. The most confusing issue during such a classification is a variety of land covers that make vague land classes. The Fusion of Optical SAR Satellite data merges more data from the satellite images than optical products.

The incorporation of spatial information, in conjunction with usual classification methods, obtains more adaptability to the scientist. Thus, an efficient classification technique should be used, and

reliable features should be derived from multiple sources in the case of urban area mapping with spectrally similar or mixed classes.

Comparing the exactness of the results were applied in different methods in this research, indicates that the combination of 4-bands, NDVI, $\Delta$HH, mean HV, mean HH have the highest accuracy.

# Chapter 5

# General conclusions

In recent years, increase in data accessibility, and advances in satellite technology have diversified the use of remote sensing for mapping and monitoring natural hazards and land cover classification and changes. An advantageous application of remote sensing in a wide range, including the detection of earthquakes damage, study about faults and volcanic activity, monitoring landslides and flooding have proven.

In this study, official statistical data, field survey data, and multi-temporal satellite imagery have been used to evaluate the reconstruction process and land cover changes in the city of Bam after it was struck by a devastating earthquake on December 26, 2003. The study's significance lies in its use of satellite images and remote sensing technologies that have not previously been applied in studies conducted on Bam. Furthermore, it should be noted that the reconstruction policy formulated for Bam not only responded to the demand for the reconstruction of residential units, but also provided social and urban development and economic growth by establishing new infrastructure, public buildings, and cultural facilities.

Our evaluation showed that reconstruction of a significant number of buildings had been completed within 2 to 3 years of the earthquake's occurrence. This indicates that the pace and progress of the reconstruction project were acceptable and that the project was conducted efficiently compared with previous governmental reconstruction projects in Iran. Moreover, a comparison of the building materials and structural types employed in Bam before and after the earthquake showed that the quality of the building structures had generally improved, probably as a result of direct supervision by the Civil Engineering Organization. It is expected that the new city of Bam will achieve greater sustainability than its predecessor while being much more resilient to future disaster events.

Our results showed that the reconstruction process was adequate in partially damaged districts of the city. However, in severely damaged areas, a sizeable area of vacant land remains despite the implementation of post-earthquake reconstruction. This can be attributed to the destruction of gardens, the deaths of their former owners, and the construction of some steel-frame buildings with smaller footprints.

In sum, we can conclude that the implementation of Bam's reconstruction plan has been successful, particularly when compared with earlier post-disaster development programs implemented in other cities in Iran. The important factors that contributed to the success of this plan were financial aid and construction materials provided by the government and the active participation of local survivors in the reconstruction process. Although the 2003 Bam earthquake resulted in extensive physical damage and loss of human lives, it led to a rise in national awareness relating to the reduction of risks associated with earthquakes and an improvement in the quality of disaster management in Iran. Finally, it should be noted that although the analysis of satellite images conducted for this study ensured high accuracy and reduced costs compared with conventional methods entailing field surveys and data collection, the process of manual classification is time-consuming and requires considerable expertise.

In the next chapter, we attempt to develop powerful algorithms to enable automatic and highly accurate detection of types of land cover. The results show, by using only the optical data, more than half of pixels relates to the soil have been wrongly realized buildings, and more than half of pixels belonging to the building have been incorrectly achieved as soil. The variety of soil type and matching their color with the color of construction materials in the buildings in this kind of desert district is the primary reason for these significant errors. To solve this difficulty we have used SAR images.

Hence, to improve the land cover classification for arid areas conditions like Bam, we applied a combination of optical and active microwave images. The optical data are also incorporated, to increase the effect of the vegetation on the SAR images and better classification of the radar data. The Fusion of Optical SAR Satellite data merges more data from the satellite images than optical products. And finally, comparing the exactness of the results were applied in different methods in this research, indicates that the combination of 4-bands, NDVI, $\Delta$HH, mean HV, mean HH have the highest accuracy.

# References

Akasheh, O.Z., C.M.U. Neale, and H. Jayanthi. "Detailed Mapping of Riparian Vegetation in the Middle Rio Grande River Using High-Resolution Multi-Spectral Airborne Remote Sensing." Journal of Arid Environments 72, no. 9 (September 2008): 1734–1744. doi:10.1016/j.jaridenv.2008.03.014.

Albaladejo, J., M. Martinez-Mena, A. Roldan, and V. Castillo. "Soil Degradation and Desertification Induced by Vegetation Removal in a Semiarid Environment." Soil Use and Management 14, no. 1 (March 1998): 1–5. doi:10.1111/j.1475-2743.1998.tb00602.x.

Allamehzadeh M, Dezvareh M, Farahbod AM, Hatzfeld D, Mokhtari M, Moradi AS, Mostafazadeh M, Paul A, Tatara M (2005) Seismological aspects of the 2003 Bam, Iran, earthquake and its aftershock analysis. Earthq Spectra 21(S1): S101–S112

Alrababah, M. A., and M. N. Alhamad. 2006. Land use/cover classification of arid and semi-arid Mediterranean landscapes using Landsat ETM. International Journal of Remote Sensing 27 (13): 2703-2718.

Amarsaikhan, D., Ganzorig, M., Ache, P. and Blotevogel, H., 2007. The Integrated Use of Optical and InSAR Data for Urban Land Cover Mapping, International Journal of Remote Sensing, 28, pp.1161-1171.

Amarsaikhan, D., Saandar, M., Ganzorig, M., Blotevogel, H.H. and Enkhjargal, D., 2012. Comparison of multisource image fusion methods and land cover classification. International Journal of Remote Sensing, 33(8), pp. 2532-2550.

Anil Z Chitade, "Color Based Image Segmentation using K-Means Clustering," International Journal of Engineering Science and Technology, Vol. 2, NO.10, p5319-5325, 2010.

Bargiel D, Herrmann S. 2011. Multi-temporal land-cover classification of agricultural areas in two European regions with high resolution spotlight Terra SAR-X data. Remote Sensing 3(5): 859-877. doi: 10.3390/rs3050859

Buenemann M, Martius C, Jones JW, Herrmann SM, Klein D, Mulligan M, Reed MS, Winslow M, Washington-Allen RA, Lal R, Ojima D. 2011. Integrative geospatial approaches for the comprehensive monitoring and assessment of land management sustainability: Rationale, potentials, and characteristics. Land Degradation & Development 22: 226–239.

Chaouch, Naira, Marouane Temimi, Scott Hagen, John Weishampel, Stephen Medeiros, and Reza Khanbilvardi. "A Synergetic Use of Satellite Imagery from SAR and Optical Sensors to Improve Coastal Flood Mapping in the Gulf of Mexico." Hydrological Processes 26, no. 11 (September 28, 2011): 1617–1628. doi:10.1002/hyp.8268.

Chehbouni, A. "Estimation of Heat and Momentum Fluxes over Complex Terrain Using a Large Aperture Scintillometer." Agricultural and Forest Meteorology 105, no. 1–3 (November 20, 2000): 215–226. doi:10.1016/s0168-1923(00)00187-8.

Chen, X., L. Vierling, and D. Deering. 2005. A simple and effective radiometric correction method to improve landscape change detection across sensors and across time. Remote Sensing of Environment 98 (1): 63-79.

Chiroiu L (2005) Damage assessment of the 2003 Bam, Iran, earthquake using ikonos imagery. Earthq Spectra 21(S1): S219–S224

Congalton, R. G. 1991. A review of assessing the accuracy of classifications of remotely sensed data. Remote Sensing of Environment 37 (1): 35-46.

Congalton, R. G., and K. Green. 2009. Assessing the accuracy of remotely sensed data: principles and practices. 2nd ed. Boca Raton, FL: Taylor & Francis Group.

Coppin, P., I. Jonckheere, K. Nackaerts, B. Muys, and E. Lambin. 2004. Digital change detection methods in ecosystem monitoring: A review. International Journal of Remote Sensing 25 (9): 1565-1596.

Dell'Acqua, F., 2009. The role of SAR sensors. In P. Gamba, & M. Herold (Eds.), Global mapping of human settlements: Experiences, data sets, and prospects, pp. 209–319.

Demircan, A., M. Rombach, and W. Mauser. "Extraction of Soil Moisture from Multitemporal, ERS-1 SLC Data of the Freiburg Test-Site." Proceedings of IGARSS '93 - IEEE International Geoscience and Remote Sensing Symposium (n.d.). doi:10.1109/igarss.1993.322414.

Du, Y., P. M. Teillet, and J. Cihlar. 2002. Radiometric normalization of multitemporal high-resolution satellite images with quality control for land cover change detection. Remote Sensing of Environment 82: 123-134.

DUTTA, Dushmanta, Srikantha HERATH, and Katumi MUSIAKE. "DISTRIBUTED HYDROLOGIC MODEL FOR FLOOD INUNDATION SIMULATION." PROCEEDINGS OF HYDRAULIC ENGINEERING 43 (1999): 25–30. doi:10.2208/prohe.43.25.

Ellis, E., and R. Pontius. 2010. Land-use and land-cover change. In: Encyclopedia of Earth. Eds. Cutler J. Cleveland (Washington, D.C.: Environmental Information Coalition, National Council for Science and the Environment). http://www.eoearth.org/article/Land-use_and_land-cover_change

Elmore, A., J. Mustard, S. J. Manning, and D. B. Lobell. 2000. Quantifying vegetation change in semiarid environments precision and accuracy of Spectral Mixture Analysis and the Normalized Difference Vegetation Index. Remote Sensing of Environment 73 (1): 87-102.

Erener, E., 2013. Classification method, spectral diversity, band combination and accuracy assessment evaluation for urban feature detection. International Journal of Applied Earth Observation and Geoinformation, 21, pp. 397–408.

Escadafal, R., F. Albinet, and V. Simonneaux. 2005. Arid Land cover change trend analysis with series of satellite images for desertification monitoring in Northern Africa. In International Symposium on Remote Sensing of the Environment. Global monitoring for sustainability and security.

Eshghi S, Zare M, Naser Asadi K, Seyed Razzaghi M, Noorali Ahari M, Motamedi M (2004) Reconnaissance report on 26 December 2003 Bam earthquake. International Institute of Earthquake Engineering and Seismology (IIEES), Tehran, Iran

FAOSTATS (2011). Food and Agriculture Organization of the United Nations. http://faostat.fao.org/.

Foody, G. M., and A. Mathur. 2004. A relative evaluation of multiclass image classification by support vector machines. IEEE Transactions on Geoscience and Remote Sensing 42 (6): 1335-1343.

Furby, S. L., and N. A. Campbell. 2001. Calibrating images from different dates to "like-value" digital counts. Remote Sensing of Environment 77: 186 - 196.

Galletti, Christopher, and Soe Myint. "Land-Use Mapping in a Mixed Urban-Agricultural Arid Landscape Using Object-Based Image Analysis: A Case Study from Maricopa, Arizona." Remote Sensing 6, no. 7 (June 30, 2014): 6089–6110. doi:10.3390/rs6076089.

Gao, J. 2008. Detection of changes in land degradation in northeast China from Landsat TM and ASTER data. In The International Archives of the Photogrammetry, Remote Sensing and Spatial Information Sciences. Vol. XXXVII. Part B7. Beijing 2008.

Giri, Chandra. "Remote Sensing of Land Use and Land Cover." Remote Sensing Applications Series (May 17, 2012). doi:10.1201/b11964

Ghafory-Ashtiany M, Hosseini M (2007) Post-Bam earthquake: recovery and reconstruction. Nat Hazards 44:229–241

Gomez-Chova L, Calpe J, Camps-Valls G, Martin JD, SoriaE, Vila J, Alonso-Chorda LMoreno J. 2003. Feature selection of hyperspectral data through local correlation and SFFS for crop classification. In Geoscience and Remote Sensing Symposium proceedings. 21-25 July, France, Vol. 1, pp. 555-557. doi: 10.1109/IGARSS.2003.1293840

Gu¨nthal G (ed) (1998) European Macroseismic Scale 1998 (EMS-98). Cahiers du Centre Europe´en de Ge´odynamique et de Se´ismologie 15, Centre Europe´en de Ge´odynamique et de Se´ismologie, Luxembourg, 99 pp

Gusella L, Adams BJ, Bitteli CK, Huyck CK, Mognol A (2005) Object-oriented image understanding and post-earthquake damage assessment for the 2003 Bam, Iran, earthquake. Earthq Spectra 21(S1): S225– S238

Hadjimitsis, D. G., G. Papadavid, A. Agapiou, K. Themistocleous, M. G. Hadjimitsis, and A. Retalis. 2010. Atmospheric correction for satellite remotely sensed data intended for agricultural applications_: impact on vegetation indices. Natural Hazards and Earth System Science (10): 89-95.

Harris, R. "Remote Sensing of Agriculture Change in Oman." International Journal of Remote Sensing 24, no. 23 (January 2003): 4835–4852. doi:10.1080/0143116031000068178.

Hashemi-Parast, S. Omid, Fumio Yamazaki, and Wen Liu. "Monitoring and Evaluation of the Urban Reconstruction Process in Bam, Iran, after the 2003 Mw 6.6 Earthquake." Natural Hazards 85, no. 1 (September 1, 2016): 197–213. doi:10.1007/s11069-016-2573-9.

Henry, L.A., & Douhovnikoff, V. (2008). Environmental issues in Russia. Annual Review of Environment and Resources, 33, 437-460.

Hill, A. A., Keys-Mattews, L. D., Adams, B. J., & Podolsky, D. (2006). Remote sensing and recovery: a case study on the Gulf Coast of the United States. In Proceedings of the 4th International Workshop on Remote Sensing for Disaster Response (Cambridge, United Kingdom).

Hisada Y, Shibaya A, Ghayamghamian MR (2004) Building damage and seismic intensity in Bam city from the 2003 Iran, Bam, earthquake. Bull Earthq Res 79:81–93

JICA (2013) The study of reconstruction processes from large-scale disasters, JICA's support for reconstruction, final report. Japan International Cooperation Agency, EI, JR, pp 13–250

Houet T, Loveland TR, Hubert-Moy L, Gaucherel C, Napton D, Barnes CA and Sayler KL (2009) Exploring subtle land use and land cover changes: a framework for future landscape studies, Landscape Ecology (this issue) http://dx.doi.org/10.1007/s10980-009-9362-8

Hu, S. and Wang, L., 2013. Automated urban land-use classification with remote sensing. International Journal of Remote Sensing, 34(3), pp. 90–803.

Idol, Terry, Barry Haack, and Ron Mahabir. "An Evaluation of Radarsat-2 Individual and Combined Image Dates for Land Use/Cover Mapping." Geocarto International 31, no. 10 (December 28, 2015): 1108–1122. doi:10.1080/10106049.2015.1120351.

Jensen JR. 2005. Thematic information extraction: pattern recognition. In Introductory Digital Image Processing: A Remote Sensing Perspective. 3rd edited by C.C. Keith, Prentice Hall Series in Geographic Information Science, Saddle River, NJ, USA, pp.337–406.

KATO, Keita, and Fumio YAMAZAKI. "Detection of Flooded Areas Using ALOS/PALSAR Images for the 2008 Iwate-Miyagi Inland Earthquake." Journal of Japan Association for Earthquake Engineering 10, no. 3 (2010): 1–11. doi:10.5610/jaee.10.3_1.

Kitamoto A, Andaroodi E, Matini M, Ono K (2011) Post-disaster reconstruction of cultural heritage: Citadel of Bam, Iran. Proceeding of IPSJ SIG computers and the humanities symposium, Kyoto, pp 11–18, 2011–12

Kohiyama M, Yamazaki F (2005) Damage detection for 2003 Bam, Iran, earthquake using Terra-ASTER satellite imagery. Earthq Spectra 21(S1): S267–S274

Kundzewicz, Z.W., D. Rosbierg, S.P. Simonovic andK. Takeuchi, 1993. Extreme Hydrological Events: Precipitation, Floods, and Droughts. IAHSPublication, No.213, pp: 21-32

Lanza, L. and M. Conti, 1994. Remote Sensing and GIS: Potential Application for Flood Hazard Forecasting.EGIS. Retrieved from: http://www.odyssey.maine.edu/gisweb/spatdb/egis/eg94208.html.

Le Hegarat-Mascle, S, Quesney A, Vidal-Madjar D, Taconet O, Normand M, Loumagne C. 2000. Land cover discrimination from multitemporal ERS images and multispectral Landsat images: a study case in an agricultural area in France.

Leprieur, C., Kerr, Y. H., Mastorchio, S., and J. C. Meunier, 2000, "Monitoring Vegetation Cover Across Semi-arid Regions: Comparison of Remote Observations from Various Scales," International Journal of Remote Sensing, 21:281–300.

Li, L., S. Ustin, and M. Lay. 2005. Application of AVIRIS data in detection of oil-induced vegetation stress and cover change at Jornada, New Mexico. Remote Sensing of Environment 94 (1): 1-16.

Liu, W., and Yamazaki, F., Gokon, H., 2012, Damage Detection of the 2011 Tohoku, Japan Earthquake from High-resolution SAR Intensity Images, 15WCEE.

Liu, W., Matsuoka, M., Yamazaki, F., Nonaka, T., Sasagawa, T., 2014, Detection Of Building Sidewall Damage Caused By The 2011 Tohoku, Japan Earthquake Tsunamis using High-resolution SAR imagery, Tenth U.S. National Conference on Earthquake Engineering Frontiers of Earthquake Engineering.

Liu, X, Bo Y. 2015. Object-based crop species classification based on the combination of airborne hyperspectral images and LiDAR data. Remote Sensing7(1): 922- 950.doi:10.3390/rs70100922

Lo, Tommy Y., and K.T.W. Choi. "Building Defects Diagnosis by Infrared Thermography." Structural Survey 22, no. 5 (December 2004): 259–263. doi:10.1108/02630800410571571.

Lu, D., and Q. Weng. 2007. A survey of image classification methods and techniques for improving classification performance. International Journal of Remote Sensing 28 (5): 823-870.

Maghsoudi Y, Collins M, Leckie D. 2012. Speckle reduction for the forest mapping analysis of multi-temporal Radarsat-1 images. International Journal of Remote Sensing 33(5): 1349-1359. doi:10.1080/01431161.2011.568530

Mahdi T, Mahdi A (2013) Reconstruction and retrofitting of buildings after recent earthquakes in Iran. Procedia Eng 54: S127–S139

Mildrexler, David J., Maosheng Zhao, and Steven W. Running. "Where Are the Hottest Spots on Earth?" Eos, Transactions American Geophysical Union 87, no. 43 (October 24, 2006): 461–467. doi:10.1029/2006eo430002.

Murao, H., Yamamoto, K., Matsuda, S. et al. J Bone Miner Metab (2013) 31: 390. doi:10.1007/s00774-013-0429-x

Murao O, Hoshi T, Estrada M, Sugiyasu K, Matsuoka M, Yamazaki F (2013) Urban recovery process in Pisco after the 2007 Peru earthquake. J Disaster Res 8(2):356–364

Nadim F, Moghtaderi-Zadeh M, Lindholm C, Andresen A, Remseth S, Bolourchi MJ, Mohtari M, Tvedt E (2004) The Bam earthquake of 26 December 2003. Bull Earthq Eng 2:119–153

NASA Science Mission Directorate Earth Science Division. 2007. NASA Earth science requirements for suborbital observations.

Nicholson, Sharon E. "Defining Aridity: The Classification and Character of Dryland Climates." Dryland Climatology (n.d.): 151–161. doi:10.1017/cbo9780511973840.013.

Niel TG, and McVicar TR. 2004. Determining temporal windows for crop discrimination with remote sensing: a case study in south-eastern Australia. Computers and Electronics in Agriculture 45(1): 91 108.doi:10.1016/j.compag.2004.06.003

OAS (1990). Disaster, Planning, and Development: Managing Natural Hazards to Reduce Loss. Dept. Regional Development and Environment. Organization of American States. Washington, USA, 80.

Okin, G. S., and D. A. Roberts. 2004. Remote sensing in arid regions: challenges and opportunities. In Remote Sensing for Natural Resources Management and Environmental Monitoring, ed. S.L. Ustin, 111-136. Hoboken, NJ: John Wiley & Sons, Inc.

Omidvar B, Zafari H, Khakpour M (2011) Evaluation of public participation in reconstruction of Bam, Iran, after the 2003 earthquake. Nat Hazards 59:1397–1412. doi:10.1007/s11069-011-9842-4

Pacifici, F., Chini, M., and Emery. J., 2009. A neural network approach using multi-scale textural metrics from very high-resolution panchromatic imagery for urban land-use classification. Remote Sensing of Environment, 113, pp. 1276–1292.

POHL, C. and VAN GENDEREN, J.L., 1998, Multisensor image fusion in remote sensing: concepts, methods, and applications. International Journal of Remote Sensing, 19, pp. 823-854.

Pooyan Z (2012) Earthquake recovery experiences: some principles toward sustainability. Proceedings of the 15th world conference on earthquake engineering, Lisbon, 2012-09-24/2012-09-28

Rathje EM, Crawford M, Woo K, Neuenschwander A (2005) Damage patterns from satellite images of the 2003 Bam, Iran, earthquake. Earthq Spectra 21(S1): S295–S308

Rawat, J. S., & Kumar, M. (2015). Monitoring land use/cover change using remote sensing and GIS techniques: A case study of Hawalbagh block, District Almora, Uttarakhand, India. The Egyptian Journal of Remote Sensing and Space Science, 18(1), 77-84.

Rhee, J., Im, J., & Carbone, G. J. (2010). Monitoring agricultural drought for arid and humid regions using multi-sensor remote sensing data. Remote Sensing of Environment, 114(12), 2875–2887. doi:10.1016/j.rse.2010.07.005

Richards, John A., and Xiuping Jia. "Feature Reduction." Remote Sensing Digital Image Analysis (1999): 239–257. doi:10.1007/978-3-662-03978-6_10.

Roychowdhury, K. "COMPARISON BETWEEN SPECTRAL, SPATIAL AND POLARIMETRIC CLASSIFICATION OF URBAN AND PERIURBAN LANDCOVER USING TEMPORAL SENTINEL – 1 IMAGES." ISPRS - International Archives of the Photogrammetry, Remote Sensing and Spatial Information Sciences XLI–B7 (June 22, 2016): 789–796. doi:10.5194/isprs-archives-xli-b7-789-2016.

Sabins, F.F., 1986. Remote Sensing: Principles and Interpretations. W.H. Freeman. New York.

Sandberg, M., Rauste, Y., Häme, T. & Antropov, O. 2015. "Land cover mapping with multitemporal C-band SAR and optical satellite data in the boreal forest zone". In: International Geoscience and Remote Sensing Symposium (IGARSS), submitted, 2015.

Sawaya S, Haack B, Idol T, Sheoran A. 2010. Land use/cover mapping with quad-polarization RADAR and derived texture measures near Wad Madani, Sudan. GIScience and Remote Sensing 47(3): 398-411. doi: 10.2747/1548-1603.47.3.398

Schroeder, T. A., W. B. Cohen, C. Song, M. J. Canty, and Z. Yang. 2006. Radiometric correction of multi-temporal Landsat data for characterization of early successional forest patterns in western Oregon. Remote Sensing of Environment 103: 16-26.

Short, N. M.. 2010. The Remote Sensing Tutorial. NASA, National Aeronautics and Space Administration. http://rst.gsfc.nasa.gov/ (last accessed 7 July 2016).

Shupe, Scott M., and Stuart E. Marsh. "Cover- and Density-Based Vegetation Classifications of the Sonoran Desert Using Landsat TM and ERS-1 SAR Imagery." Remote Sensing of Environment 93, no. 1–2 (October 2004): 131–149. doi:10.1016/j.rse.2004.07.002.

Small, C. 2002. Multitemporal analysis of urban reflectance. Remote Sensing of Environment 81 (2-3): 427-442.

Song, C., C. E. Woodcock, K. C. Seto, M. P. Lenney, and S. A. Macomber. 2001. Classification and change detection using Landsat TM data_: When and how to correct atmospheric effects? Remote Sensing of Environment 75 (2): 230-244.

Statistical Center of Iran (2004) Bam Earthquake Statistical Survey, 2004 (Online). http://amar.sci.org.ir/ Detail.aspx?Ln=F&no=201629&S=GW

Statistical Center of Iran (2011) Implementation of the 2011 Iranian Population and Housing Census in autumn (24 October–13 November 2011), 2011 (Online). http://www.amar.org.ir/Default.aspx?tabid= 765

Stavrakoudis, D.G., Theocharis, J.B. and Zalidis, G.C., 2011. A Boosted Genetic Fuzzy Classifier for land cover classification of remote sensing imagery. ISPRS Journal of Photogrammetry and Remote Sensing, 66, pp. 529–544.

Stefanski J, Kuemmerle T, Chaskovskyy O, Griffiths P, Havryluk V, Knorn J, Waske B. 2014. Mapping land management regimes in Western Ukraine using optical and SAR data. Remote Sensing 6(6): 5279-5305.doi:10.3390/rs6065279

Taubenböck, H., Esch, T., Felbier, A., Wiesner, M., Roth, A. and Dech, S., 2012. Monitoring urbanization in mega cities from space. Remote Sensing of Environment, 117, pp. 162-176.

Teillet, Philippe M., and Craig A. Coburn. "Radiometric Correction." Encyclopedia of Geography. 2010. SAGE Publications. 4 Oct. 2010.

Tou, J. T. and R. C. Gonzalez, 1974. Pattern Recognition Principles, Addison-Wesley Publishing Company, Reading, Massachusetts.

Turner MD, Congalton RG. 1998. Classification of multi-temporal SPOT-XS satellite data for mapping rice fields on a West African floodplain. International Journal of Remote Sensing, 19(1): 21–41. doi:10.1080/014311698216404

UNDRO (1991). Mitigating Natural Disasters. Phenomena, Effects, and Options. United Nations Disaster Relief Coordinator, United Nations, New York, 164.

Van Westen, C. J. (2000). Remote sensing for natural disaster management. International Archives of Photogrammetry and Remote Sensing, 33(B7/4; PART 7), 1609-1617.

Van Leeuwen, W.J.D., A.R. Huete, S. Jia, and C.L. Walthall. "Comparison of Vegetation Index Compositing Scenarios: BRDF Versus Maximum VI Approaches." IGARSS '96. 1996 International Geoscience and Remote Sensing Symposium (n.d.). doi:10.1109/igarss.1996.516685.

Xie, Y., Z. Sha, and M. Yu. 2008. Remote sensing imagery in vegetation mapping: a review. Journal of Plant Ecology 1 (1): 9-23.

Xu, H. 2010. Analysis of impervious surface and its impact on urban heat environment using the Normalized Difference Impervious Surface Index (NDISI). Photogrammetric Engineering & Remote Sensing 76 (5): 557-565.

Yamazaki F, Yano Y, Matsuoka M (2005) Visual damage interpretation of buildings in Bam City using QuickBird images following the 2003 Bam, Iran, earthquake. Earthq Spectra 21(S1):S329–S336

Yang, L., G. Xian, J. M. Klaver, and B. Deal. 2003. Urban land-cover change detection through sub-pixel impervious mapping using remotely sensed data. Photogrammetric Engineering & Remote Sensing 69 (9): 1003-1010.

Yekkehkhany B, Homayouni S, McNairn H, Safari A. 2014. Multi-temporal full polarimetry L-band SAR data classification for agriculture land cover mapping, Geoscience and Remote Sensing Symposium pp. 2770-2773. doi: 10.1109/IGARSS.2014.6947050

Zubair, A. O. (2006). Change detection In land use and land cover using remote sensing data and GIS. A case study of Ilorin and its environs in Kwara, State. Bogenrieder, A. Das Schilfrohr (Phragmites australis (Cav.) Trin). Biol. Unserer Zeit 1990, 20, 221–222.